TU DELFT

Evaluation of transport properties of radionuclides in clay materials

Master Thesis

Yifan Wu

8/28/2017

Feasibility study of Dutch concept of deep geological repository for radioactive waste is at present widely conducted in the Netherlands. In this project, transport properties of selenate ion in clay materials were investigated. Apparent diffusion coefficients of selenate ion were obtained as results. To study possible alternations of Boom Clay by alkaline concrete pore water, elemental composition and pore structure of raw Boom Clay samples were characterized.

Evaluation of transport properties of radionuclides in clay materials

Yifan Wu
4470214

Master thesis performed at:

Section Reactor Physics and Nuclear Materials
Radiation Science and Technology
Reactor Institute Delft
Delft University of Technology

Under supervision of:

Dr. Denis Bykov
Dr. Andrea Sabau

Graduation Committee:

Prof. Joris Dik
Dr. Denis Bykov
Dr. Danny Lathouwers
Dr. Andrea Sabau
Dr. Anne-Catherine Dieudonné

28th August, 2017

Acknowledgements

In spite of a lot of difficulties encountered, the thesis project of mine finally is coming to an end successfully. During the process of finding solutions to problems in experiments, skills of critical thinking and problem solving of mine were enhanced. Furthermore, during investigations of this topic, certain experimental skills and characterization techniques were cultivated, thanks to patient guidance from Dr. Denis Bykov and Dr. Andrea Sabau.

At the end of this project, I am glad to see that a series of reliable experimental data has been obtained, and with further investigations I believe valuable suggestions could be given on the future construction of Dutch deep geological repository for radioactive waste.

I would like to thank all laboratory staff and members of section Reactor Physics and Nuclear Materials (RPNM) for continuously supporting me during my work at the Reactor Institute Delft.

I would like to also thank my home faculty Materials Sciences and Engineering (MSE) for giving me support during study, examinations and graduation.

I would like to thank the teachers who have great passion in their research areas and patient guidance towards students, for inspiring us.

Thanks to all my graduation committee members for giving me valuable advice and suggestions.

At last, I have been troubled by anxiety for a long time, I would not be able to come to this end without care and support from my family, my friends and my supervisors. I like to give my appreciations to them as well.

Contents

1. Context of the study: Introduction

Since the first reactor launched by Fermi's group in 1942, the utilization of nuclear energy has been developing in an extremely rapid pace. After seven decades of development, there are already 447 operable nuclear reactors all over the world by 1st August, 2017 according to World Nuclear Association (WNA) and power generated takes up to 10.6% of the total global power generation by 2016 according International Atomic Energy Agency (IAEA) [1]. However, as an unavoidable product of nuclear reactions, radioactive waste is one of the most vital issues to be considered along with the development of nuclear energy.

Six classes of waste were defined by IAEA on the basis of the activity and the half-life of radioactive waste: exempt waste (EW), very short lived waste (VSLW), very low level waste (VLLW), low level waste (LLW), intermediate level waste (ILW) and high level waste (HLW) [2]. Among these, high level waste usually consists of activation products, actinides and fission products, which are respectively dominant at different stages of service. After 100-year service, ^{137}Cs, ^{90}Sr and their short-lived daughters are dominant species; after 1000-year service, the actinides are dominant; and during period between 10000- and 100000-year service, activation products, actinides and fission products are all vital species [3]. Due to high risk caused by HLW, it is required to be permanently stored in a proper environment distant away from biosphere. Several disposal measures have been considered and investigated by a lot of countries, including: near-surface disposal, deep geological disposal, long-term above ground storage, disposal in outer space, rock-melting, disposal at subduction zones, sea disposal, sub seabed disposal, disposal in ice sheets, direct injection, etc [4-6]. Among these, deep geological disposal is widely acknowledged as the most effective and secure measure for ILW and HLW.

Deep geological disposal takes advantage of the inherent isolating properties of bedrock, accompanied with several engineered barriers, to keep ILW or HLW securely away from biosphere. Such structure of deep geological repositories has been conceived of and designed by quite a few research institutes from Belgium, Canada, China, Czech, Finland, France, Germany, Japan, Netherlands, Spain, Sweden, Switzerland, United Kingdom, United State of America, etc [7-18]. Compared to other European countries, the study of radioactive waste disposal in the Netherlands is at an early conceptual phase [19]. The current policy in the Netherlands is an interim storage of all the radioactive waste for a period of at least 100 years at the waste management organisation COVRA, to perform research preferably in international collaborative programs and eventually to dispose all radioactive waste retrievably in a deep geological facility [19].

The Dutch research programme OPERA was dedicated to investigating the disposal of radioactive waste in clay and the design of a deep geological repository. A general

concept of the repository has been described in Verhoef et al [19]. The conceptual structure of the repository consists of a sequence of natural and/or artificial barriers, as shown in Figure 1-2. Between radioactive waste and biosphere, complete isolation of toxic waste is realized by layers of metal canister, buffer material, and host rock. The choices of host rock vary with geologic features of different regions or countries [20-25]. Clay rock, salt rock, granite, crystalline rock, sedimentary rock and tuff are all considered candidates for host rock. In Dutch concept of repository structure, concrete and bentonite were chosen as the potential buffer/backfill materials, Boom Clay was chosen as the host rock because of its wide distribution over the country and its promising properties. Advantages of clay rock as host rock for geological disposal of radioactive waste include: low permeability and low hydraulic gradients, chemical buffering capacity, propensity for plastic deformation and self-sealing of fractures, low solubility of radionuclides and high retardation of the migration of radionuclides [26].

In spite of all promising properties Boom Clay may possess, effectiveness and reliability have to be examined through experimental work. In this thesis, the transport properties of buffer material bentonite and host rock Boom Clay were investigated and discussed. Comparison with results from other researchers and results of different choices of host rock will be concluded as well.

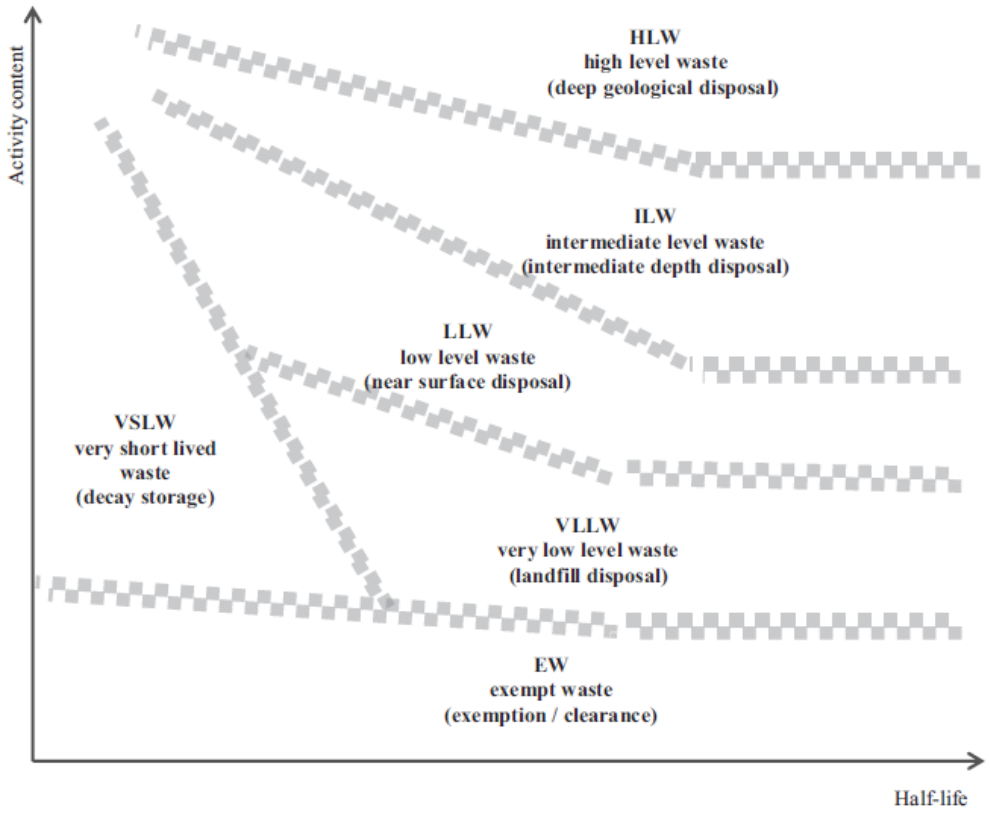

Figure 1-1: Classification of radioactive waste by IAEA definition [2].

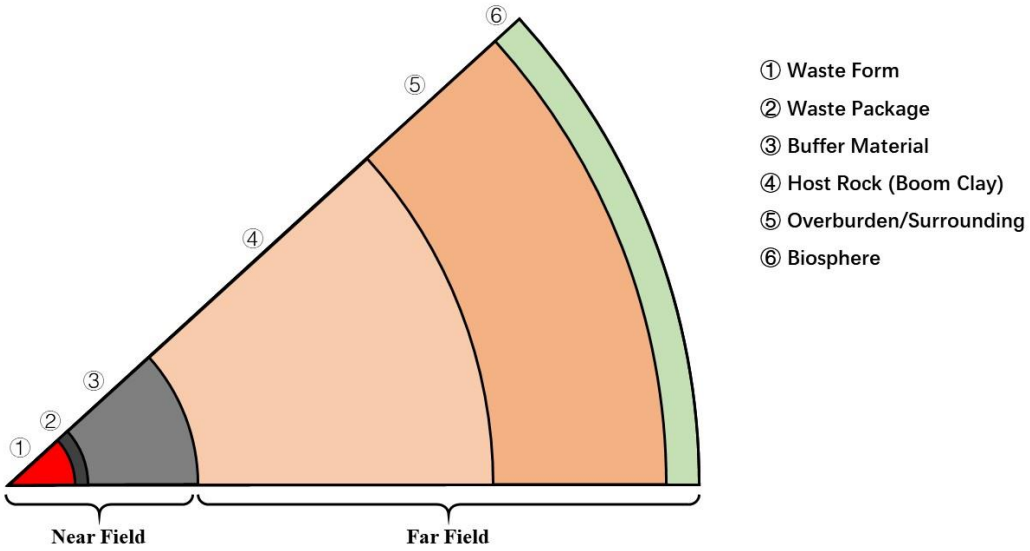

Figure 1-2: Schematic representation of multi-barrier structure of deep geological repository [19].

2. Characteristics of clay

Bentonite, derived from volcanic ash, is well acknowledged by researchers as one of the best buffer/backfill materials for protecting waste package materials (e.g. metal canisters) in deep geological repository structures [27]. The most important reason for that is montmorillonite, a member of smectite mineral group, which is present in bentonite and is accountable for to its high swelling capacity. MX-80 bentonite adopted in this project is mainly composed of Na montmorillonite.

The Belgium Boom Clay Formation, which is approximately equivalent to the Rupel Clay Member in the Netherlands and the Ratingen and Lintfort Members in Germany, is a clay-rich Oligocene marine sedimentary that is widely distributed in the northern Belgium [28, 29]. It is considered as a potential host rock for radioactive waste disposal and has been investigated for decades for its mechanical, physico-chemical and hydrogeological properties.

2.1 Characteristics of bentonite

2.1.1 Chemical composition of bentonite

Characterization of chemical composition of bentonite MX-80 was carried out in [30] by standard ICP/AES analysis. The average results are listed below:

Table 2-1: Chemical composition of bentonite MX-80 according to [30].

Component	Weight percentage (wt%)
SiO_2	67.4
Al_2O_3	21.2
Fe_2O_3	4.14
MgO	2.61
Na_2O	2.25
CaO	1.46
K_2O	0.55
TiO_2	0.17
P_2O_5	0.05
C	0.36
S	0.34
LOI	9.90

2.1.2 Mineralogical composition of bentonite

Powder bentonite samples with random crystal orientations were analysed by standard X-ray diffraction by Karnland [30]. The average mineralogical composition is given

below:

Table 2-2: Mineralogical composition of bentonite MX-80 [30].

Phase	Weight percentage (wt%)
Montmorillonite	81.4
Tridymite	3.8
Plagioclase	3.5
Muscovite	3.4
Quartz	3.0
Cristobalite	0.9
Gypsum	0.9
Illite	0.8
Pyrite	0.6
Calcite	0.2

As is well proven by various researchers [27, 30, 31], bentonite is mostly composed of montmorillonite, either of sodium type or of calcium type. According to the results from Karnland [30], approximately 81.4% of bentonite samples analysed is montmorillonite, with other accessory minerals (tridymite, plagioclase, muscovite, quartz, etc.) existing in relatively small amounts. As a buffer material, a range of 75 to 90 percent of montmorillonite content is often required. With regard to the content of typical accessory minerals, no accurate limits have been specified.

2.2 Characteristic of Boom Clay

2.2.1 Physical characteristics of Belgian Boom Clay

General physical characteristics of Belgian Boom Clay were investigated by several researchers and is summarised in Table 2-3 below. Slight divergence can exist between Belgian and Dutch Boom Clay.

Table 2-3: Physical parameters of Boom Clay [32-34].

Parameter	Unit	Value
Bulk density (sat.)	t/m^3	1.9-2.1
Average grain density	t/m^3	2.65
Water content	% dry wt	19-24
Total porosity	vol. %	36-40
Specific surface	m^2/g	44
Thermal conductivity	W/(m·K)	1.68
Specific Heat	J/(kg·K)	1400

Hydraulic conductivity Lab experiments In situ field testing	m/s	 Vert. 1.8-3.4E-12; Horiz. 3.5-7.9E-12 Vert. 2.1E-12; Horiz. 4.5E-12

2.2.2 Mineralogical composition of Belgian Boom Clay

As a representative of sedimentary rocks, Boom Clay normally consists of clay minerals, siliciclastics, accessory minerals and organic matter [29]. Quantitative and semi-quantitative analyses of clay composition are mainly conducted by X-ray diffraction (XRD) while dual range Fourier Transform Infrared Spectroscopy (FT-IR) as an alternative technique is also suitable for clay characterization [35].

In accordance with Volckaert et al. [34], a summary of mineralogical composition of Belgian Boom Clay is given in Table 2-4 below. Some of the data have been updated by recent researches by Van Keer and De Craen [36, 37].

Table 2-4: Mineralogical composition of Boom Clay [34, 36, 37].

Clay minerals Illite Smectite + illite-smectite Kaolinite Chlorite Chlorite-smectite	30-60% 10-45% 10-30% 5-20% 0-5% 0-5%
Quartz	15-60%
Feldspars Albite	1-10% 1-10%
Carbonates Calcite Siderite Dolomite Ankerite	1-5% 1-5% Present Present Present
Pyrite	1-5%
Organic carbon	1-5%
Others Glauconite, apatite, rutile, anatase, zircon, monazite, xenotime	Present

According to a series of investigations conducted, the clay mineralogy of Boom Clay, making up approximately 60% of the total composition, is dominated by illite, smectite, illite-smectite interstratifications, kaolinite and kaolinite-smectite interstratifications. Small amount of chlorite, degraded chlorite, illite-chlorite interstratifications and chlorite-smectite interstratifications also exist [29, 38]. Siliciclastics usually make up to ~30% of Boom Clay composition, consisting of quartz and feldspars. Accessory minerals usually

make up to ~8% of Boom Clay composition, consisting of carbonates, pyrite and anatase. Organic matter usually makes up to ~2% of Boom Clay composition.

2.3 Structure and properties of clay minerals

2.3.1 Structure of clay minerals

Most macroscopic properties of clay minerals are determined by the physical and chemical processes occurring microscopically at clay mineral surface. Surface properties of clay minerals are then related to crystallographic properties.

Each clay mineral has a fundamental structure consisting of one sheet of edge-sharing MO_6 octahedral (M = Al, Mg, or Fe), i.e. the octahedral sheet, combined with one or two sheets of corner-sharing MO_4 tetrahedra (M = Si or Al), i.e. the tetrahedral sheet(s). The combination of one octahedral sheet and one or two tetrahedral sheets is called a clay mineral layer (Figure 2-1). Two types of layer are defined by the number of tetrahedral sheets combined with the octahedral sheet. TO layer type is formed by 1:1 tetrahedral and octahedral sheets while TOT layer type is formed by 2:1 tetrahedral and octahedral sheets. Among common clay minerals, illite and smectite have TOT layer structures, whereas kaolinite has a TO layer structure [39].

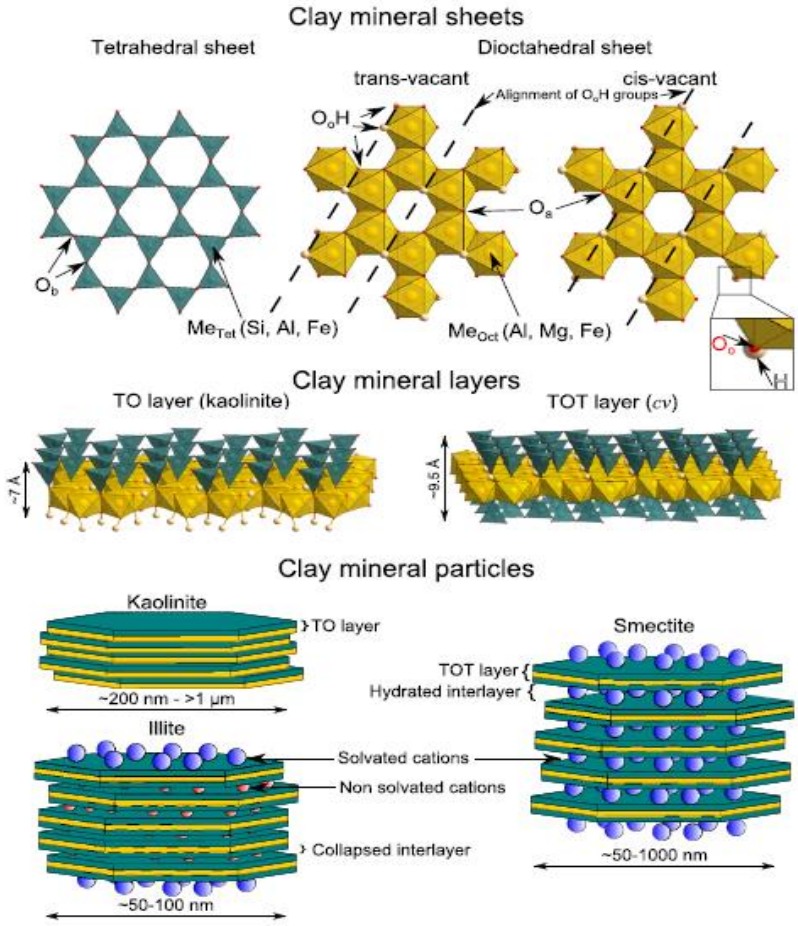

Figure 2-1: From top to bottom: tetrahedral and octahedral sheets, TO and TOT layers

and clay mineral particles [39].

The thickness of TO layers and TOT layers can be estimated by the sizes of octahedra and tetrahedra, which is about 7 Å for a TO layer and 9.5 Å for a TOT layer. However, different clay minerals display different basal plane dimensions, i.e. different aspect ratios, thus different morphologies. Layers stack to form clay mineral particles, illite particles by 5 to 20 TOT layers, kaolinite particles by 10 to 200 TO layers. For smectite, which is a swelling clay mineral, the layers can be completely delaminated [39]. These clay mineral particles can further pack together to form aggregates and aggregates assemble to become bulk clay. The volume of interlayer, interparticle and interaggregate space together makes up the total porosity of clay material.

2.3.2 Layer charge and hydration of clay minerals

Due to isomorphic substitutions of tetrahedral or octahedral metals, many clay minerals with TOT layers display a significant negative layer charge density. This negative layer charge is often balanced by ions of alkali metals (Na^+, K^+, Rb^+) and alkaline earth metals (Be^{2+}, Mg^{2+}, Ca^{2+}, Sr^{2+}). However, in clay minerals with TO layers, like kaolinite, there is no obvious positive or negative layer charge. Thus, in the interlayer region of clay mineral layers, it is either empty or occupied by charge compensating cations. In non-swelling clay minerals with negative layer charge, like illite, compensating cations are non-solvated and mostly K^+ or NH_4^+. In swelling clay minerals including smectite, interlayer compensating cations tends to be fully solvated except the cations with low hydration energies.

The amount of interlayer water varies with temperature, applied stress, the amount and origin of layer charge, the water chemical potential and the type of compensating cations [39]. At low water contents swelling of clay minerals occur in a stepwise pattern from one-layer hydrate to two-layer to three-layer and finally up to four-layer, which is termed crystalline swelling [40-42].

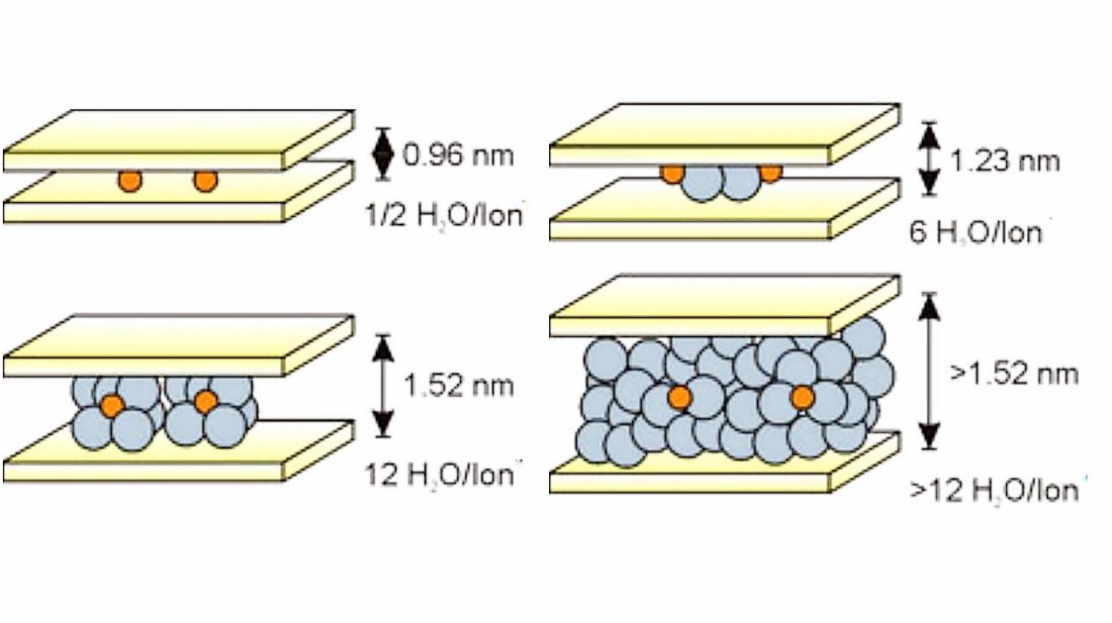

Figure 2-2: Crystalline swelling of swellable clay minerals by hydration of cations [42].

However, in Na- and Li- smectite, swelling can proceed much further with increasing water chemical potential in a continuous pattern, which is another pattern of clay mineral swelling, osmotic swelling [43]. Hydration of interlayer cations and clay surface controls the swelling, dispersion, and ion exchange properties of clays, and thus, it is an important factor affecting the usability of bentonite as a component in clay barriers.

2.3.3 Cation exchange capacity (CEC)

As was mentioned above, in clay mineral particles there often exist cations in interlayer regions or on external basal planes to compensate negative layer charge caused by isomorphic substitutions. Unless the cations are situated in collapsed interlayers of non-swelling clay minerals, these cations are easily exchangeable by other cations in solution. In non-swelling clay minerals, only the charge compensating cations on the external surfaces are available for exchange. Cation exchange capacity (CEC) of a clay mineral is defined as the total amount of charge which is balanced by exchangeable cations. The part compensating the layer structural charge (from isomorphic substitution) usually holds a constant value and is termed permanent cation exchange capacity [13].

Anion exchange capacity (AEC) shares the similar theory with cation exchange capacity, which is in turn anions compensating positive layer charge of clay particles. However, the fixation of anions is much more complicated in this case than cation exchange, in which only electrostatic force plays a role. Before 1975 anion exchange capacity was rarely investigated because the influence caused by anions is much weaker

than cation exchange in most underground environment, i.e. in temperate zones. In the following investigation by Pansu, anion exchange capacity is found much more significant in weathered soils [44]. Due to the complex essence and little influence in temperate zones of anion exchange capacity, in this project we assumed it negligible.

2.3.4 Electrical double layer (EDL)

Because of the negative layer charge of clay particles, cations adsorption on basal planes leads to anion exclusion near the clay mineral surface. To reach the equilibrium of both electrostatic force and electric neutrality, an electrical double layer formed (Figure 2-3). In the very first layer close to surface, which is termed the inner Helmholtz plane (IHP), specifically adsorbed ions are first attach to the surface by chemical interactions. Then next to IHP in the outer Helmholtz plane (OHP), counter ions are tightly bonded by electrostatic force near clay mineral surface. In the farther region from surface, the counter ions are less tightly bonded by electrostatic force. Along with thermal motion, the cations tend to move around rather than anchored firmly. Thus, this region is named diffuse layer. At different distances from the clay mineral surface, different degree of cations hydration can be observed. In the inner Helmholtz plane, there are no water molecules interposed between surface and counter ions. Hence, the counter ions stay unhydrated, the thickness of IHP is determined by the ionic radii. In the outer Helmholtz plane, there are at least one water molecules interposed, the thickness of OHP is determined by the radii of hydrated counter ions. Farther in diffuse layer, due to sufficient supply of water molecules, counter ions (cations) are all solvated and hydrated [45, 46]. Furthermore, a stagnant layer always arises formed by immobilized solvent molecules under the influence of double layer field. The viscosity of liquid near clay mineral surface will be increased due to this phenomenon and some influence on liquid migration through clay materials will be exerted.

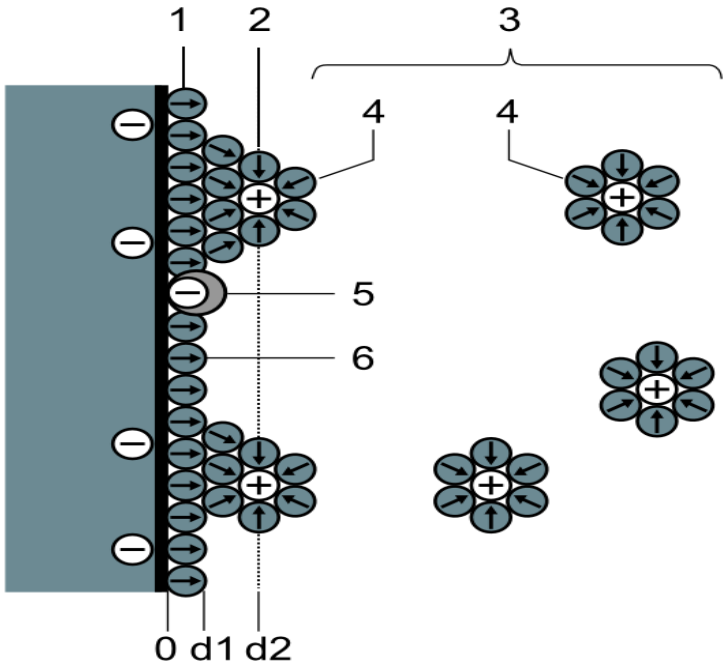

Figure 2-3: Schematic representation of a double layer based on an BDM model. [47] (1) inner Helmholtz plane (IHP); (2) outer Helmholtz plane (OHP); (3) diffuse layer; (4) solvated ions (cations); (5) specifically adsorbed ions; (6) molecules of the electrolyte solvent.

2.3.5 Sorption mechanisms

When waste package materials of radioactive waste, e.g. thick steel canisters, fail after a service of thousands of years, retention processes along the migration pathways are determinant for the safe service of the multi-barrier deep geological repository structure. Retention acts as processes that control the mobility of radionuclides released, including immobilization processes and retardation processes.

Immobilization processes are those that retain radionuclides with the barriers for an extremely long duration, usually by precipitation and co-precipitation. Retardation processes however, are processes that delay the migration of radionuclides to biosphere. Retardation processes that fix radionuclides onto mineral surfaces (of metallic oxides or clay minerals) is termed “sorption”.

Sorption processes on mineral surfaces usually occurs either forming inner-sphere complexes or outer-sphere complexes. Outer-sphere complexes are formed on planar sites of minerals by electrostatic bonding between the negatively charged mineral surface and radionuclides (mainly cations) in the interlayer regions, while inner-sphere complexes are formed on edge sites of minerals by strong covalent bonding. A schematic of inner-sphere and outer-sphere complexations is given by Marques Fernandes et al. [48] in Figure 2-4.

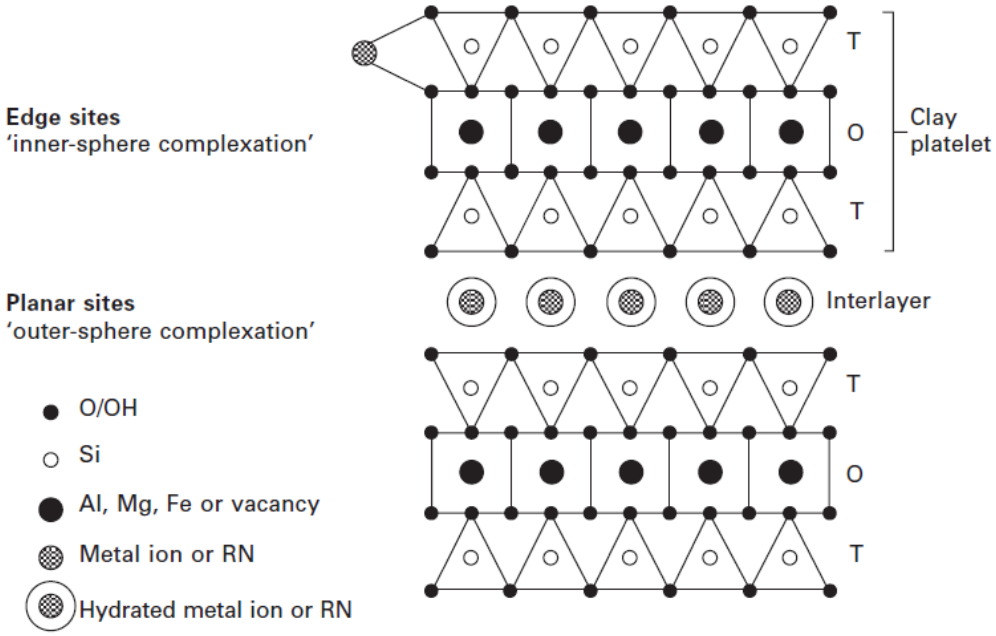

Figure 2-4: Schematic representation of sorption mechanisms [48].

The degrees and mechanisms of radionuclides sorption are determined by geochemical conditions in the aqueous environment, including pH, Eh, the inherent physical and chemical properties of radionuclides and mineral surfaces, the existence of competitive or synergetic species, etc. In outer-sphere complexations, a strong dependence on ionic strength and a weak dependence on pH are usually observed. However, in inner-sphere complexations on edge sites of mineral surfaces, a strong dependence on pH is usually observed due to the possibilities of surface protonation/deprotonation of undercoordinated oxygen atoms on the edge sites [49]. Meanwhile, a relatively weak dependence on ionic strength and a strong dependence on sorbate concentration are observed for inner-sphere complexations [48, 49].

To evaluate the degree of radionuclides sorption, the solid-liquid distribution coefficients K_d are often estimated and compared. By this distribution coefficient, the partitioning of a species between solid and aqueous phases is described, based on the assumption of a reversible equilibrium existing between dissolved and sorbed species. The definition of K_d can be given as:

$$K_d = \frac{(C_{init} - C_{eq})}{C_{eq}} \cdot \frac{V}{m} \qquad \text{(Eq. 2.1)}$$

where C_{init} is the concentration of the species in the solution before sorption, C_{eq} is the concentration of the species in the solution after sorption, V is the volume of the solution and m is the mass of solid sorbent material.

Further, deeper understanding of sorption mechanisms has been significantly increased lately by the application of various novel techniques. Particularly, synchrotron-radiation (SR) based techniques including X-ray absorption, X-ray scattering and X-ray microprobe techniques have been much more adopted due to increasing number of SR facilities available [50]. For instance, X-ray absorption spectroscopy (XAS) techniques including extended X-ray absorption fine structure (EXAFS), X-ray absorption near edge structure (XANES) and grazing incidence X-ray absorption fine structure (GIXAFS) are competent for structure characterization of bulk and surface bound radionuclides. The surface sensitive X-ray standing wave (XSW) technique is competent for characterization of atomic-scale structure of species absorbed at mineral surfaces. Microprobe techniques such as μ-XAS, μ-X-ray fluorescence spectroscopy (μ-XRF) and μ-X-ray diffraction (μ-XRD) are extremely helpful for mapping the partitioning of species in a complex system like soil or natural rocks. Apart from SR based techniques, other techniques are proven effective for complementary investigation of sorption mechanisms, like X-ray photoelectron spectroscopy (XPS), second harmonic generation (SHG), time resolved laser fluorescence spectroscopy (TRLFS), attenuated total reflection Fourier transform infrared spectroscopy (ATR-FTIR) and high-resolution transmission electron microscopy (HRTEM) [48].

2.3.6 Competitive Adsorption of Selenium Species

As introduced in the previous section, sorption of anions on clay mineral surfaces is affected by various factors including the inherent physical and chemical properties of radionuclides. Due to limited sites for surface complexation, a competition usually exists among different types of anion while dealing with complex composition of radionuclides.

Selenite ion (SeO_3^{2-}) and selenate ion (SeO_4^{2-}) are main species of selenium existing in situ. Sorption of selenite ion (SeO_3^{2-}) and selenate ion (SeO_4^{2-}) and competitive adsorption of them with other ions with similar structure, i.e. chromate (CrO_4^{2-}), molybdate (MoO_4^{2-}), sulphate (SO_4^{2-}), have been investigated by various researchers [51-54].

On γ-Al_2O_3 surface, reported by Wu et al. [53], molybdate (MoO_4^{2-}) and selenite (SeO_3^{2-}) tend to form inner-sphere complexes while chromate (CrO_4^{2-}), selenate (SeO_4^{2-}) and sulphate (SO_4^{2-}) tend to form outer-sphere complexes. Inner-sphere complexation proved to be stronger than outer-sphere complexation, a relative degree of sorption of above-mentioned anions on metal oxide surface is reported as: molybdate > selenite > selenate ~ sulphate > chromate. For strongly adsorbed anions molybdate and selenite, the prevailing specie is dependent on the relative sorption capabilities in the specific condition (pH, Eh, etc.). As for intermediately adsorbed anions chromate, selenate and sulphate, sorption of one specie is greatly suppressed by the stronger adsorbed species.

In following work of Wu et al. [53], the triple-layer model (TLM) was adopted to investigate competitive adsorption in binary systems (MoO_4^{2-}+SO_4^{2-}, MoO_4^{2-}+SeO_4^{2-}, SO_4^{2-}+SeO_4^{2-}) and a ternary system (MoO_4^{2-}+SO_4^{2-}+SeO_4^{2-}). Binary systems MoO_4^{2-}/SO_4^{2-} and MoO_4^{2-}/SeO_4^{2-} display a similarity in the results, that existence of SO_4^{2-} or SeO_4^{2-} cause no significant influence in the adsorption of MoO_4^{2-} on γ-Al_2O_3 while the adsorption of SO_4^{2-} or SeO_4^{2-} is greatly restrained by existence of MoO_4^{2-} in a certain range of pH. The reason of this result is that different surface complexation mechanisms take place in adsorption of MoO_4^{2-} and adsorption of SO_4^{2-} or SeO_4^{2-}. Sulphate ion and selenate ion are thought to have a similar adsorption affinity on metal oxide surface according to Wu et al. [51]. In the binary system of SO_4^{2-}/SeO_4^{2-}, the difference in adsorption is small. SO_4^{2-} is reported to some extent preventing SeO_4^{2-} from adsorption, while experimental data shows the opposite trend. This inconformity was attributed to oversimplification of the assumptions made in modelling. The investigation of the ternary system (MoO_4^{2-}+SO_4^{2-}+SeO_4^{2-}) displays a result agreeing with the phenomena observed in binary systems, that adsorption of SO_4^{2-} and SeO_4^{2-} are suppressed by existence of MoO_4^{2-} in a certain range of pH.

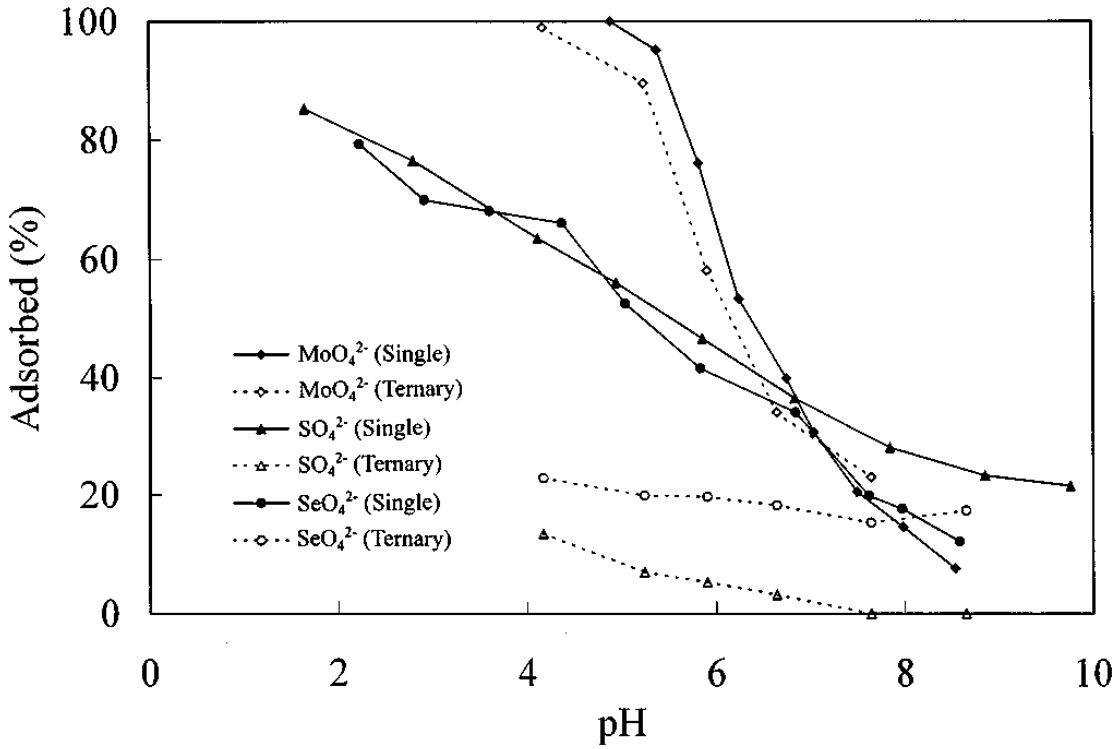

Figure 2-5: Adsorption of molybdate, sulphate and selenate on γ-Al_2O_3 surface in unary systems and in the ternary system as a function of pH [53].

In the work of Wu el al. in 2002 [52], adsorption of MoO_4^{2-}, SO_4^{2-}, SeO_4^{2-} and SeO_3^{2-} on γ-Al_2O_3 surface and adsorption of MoO_4^{2-} at various concentrations of competing specie SO_4^{2-}, SeO_4^{2-} or SeO_3^{2-} based on Freundlich equation and Langmuir equation were studied.

In unary systems of MoO_4^{2-}, SO_4^{2-}, SeO_4^{2-} and SeO_3^{2-}, parameters for adsorption process in Freundlich equation and Langmuir equation were respectively calculated.

Table 2-5: Summary of adsorption isotherm parameters calculated for the unary systems by Freundlich equation and Langmuir equation [52].

Anions	Freundlich			Langmuir		
	K	n	R^2	Q_m (μmol/g)	K (1/μmol)	R^2
MoO_4^{2-}	15.24	0.328	0.996	192.96	6.37E-3	0.915
SO_4^{2-}	28.87	0.123	0.918	80.17	1.09E-2	0.906
SeO_4^{2-}	21.43	0.179	0.944	86.03	1.50E-2	0.849
SeO_3^{2-}	24.12	0.246	0.995	164.19	1.07E-2	0.921

The Freundlich constant (n) and saturation adsorption constant Q_m are quantitative measures of the adsorption on γ-Al_2O_3 surface, displaying an accordance with previous results [51].

Investigations on the adsorption of MoO_4^{2-} at various concentrations of competing specie SO_4^{2-}, SeO_4^{2-} or SeO_3^{2-} display a trend that with increasing concentration of

competing specie less adsorption observed for MoO_4^{2-}. However, extent of competing interactions with various species can be different. Based on Sheindorf-Rebuhn-Sheintuch (SRS) equation, competition coefficients (a_{ij}) and relative affinity coefficients (α_{ij}) were calculated for binary systems MoO_4^{2-}/SO_4^{2-}, MoO_4^{2-}/SeO_4^{2-} and MoO_4^{2-}/SeO_3^{2-}.

General form of SRS equation can be expressed as:

$$q_i = K_i C_i (\sum a_{ij} C_j)^{n_i - 1} \quad \text{(Eq. 2.2)}$$

Table 2-6: Summary of competition coefficients and relative affinity coefficients for the binary systems [52].

i+j	a_{ij}	a_{ji}	α_{ij}	α_{ji}
$MoO_4^{2-}+SO_4^{2-}$	0.11	6.79	0.25	4.00
$MoO_4^{2-}+SeO_4^{2-}$	0.19	14.49	0.32	3.09
$MoO_4^{2-}+SeO_3^{2-}$	0.56	2.67	0.56	1.79

where the relative affinity coefficient was defined by Sheindorf et al. [55] and Wu et al. [51] as:

$$\alpha_{ij} = the\ overall\ proton\ coefficient\ of\ component\ j / the\ overall\ proton\ coefficient\ of\ component\ i \quad \text{(Eq. 2.3)}$$

The results showed a trend of competing interactions: $(MoO_4^{2-}+SO_4^{2-})<(MoO_4^{2-}+SeO_4^{2-})<(MoO_4^{2-}+SeO_3^{2-})$, while the values of relative affinity coefficients calculated again proved the extent of adsorption on γ-Al_2O_3 surface: $SO_4^{2-}<SeO_4^{2-}<SeO_3^{2-}<MoO_4^{2-}$.

3 Processes occurring at the interaction of Selenium with bentonite and Boom Clay

3.1 Selenium

Selenium has an electron configuration of [Ar] $3d^{10}$ $4s^2$ $4p^4$. Normally, selenium can exist in compounds or elementary substance in valence of -2 (selenide), 0 (selenium), +4 (selenite) and +6 (selenate). Se-79 is one of the most important fission products that can exist in high-level radioactive waste. Se-79 decays with β radiation with no γ radiation accompanied and has an approximate 0.327 Ma half-life as reported. Though its yield is as low as about 0.04%, it is estimated the major contribution to activity release in terms of becquerels [21]. The Pourbaix diagrams of selenium (Eh-pH diagrams) are given in Figure 3-1 according to several databases.

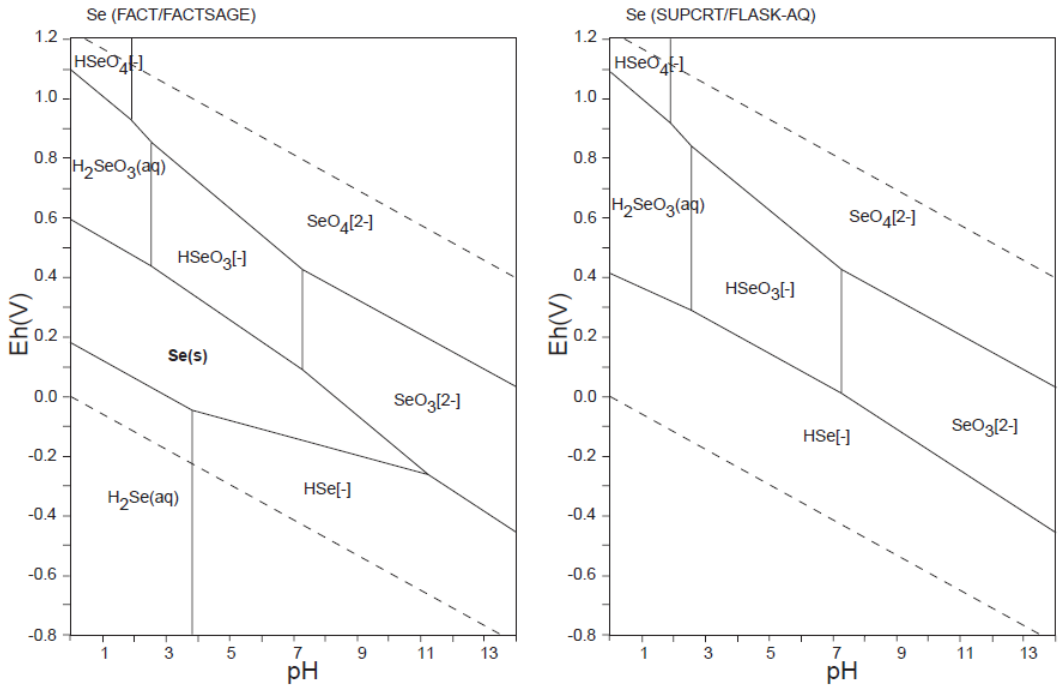

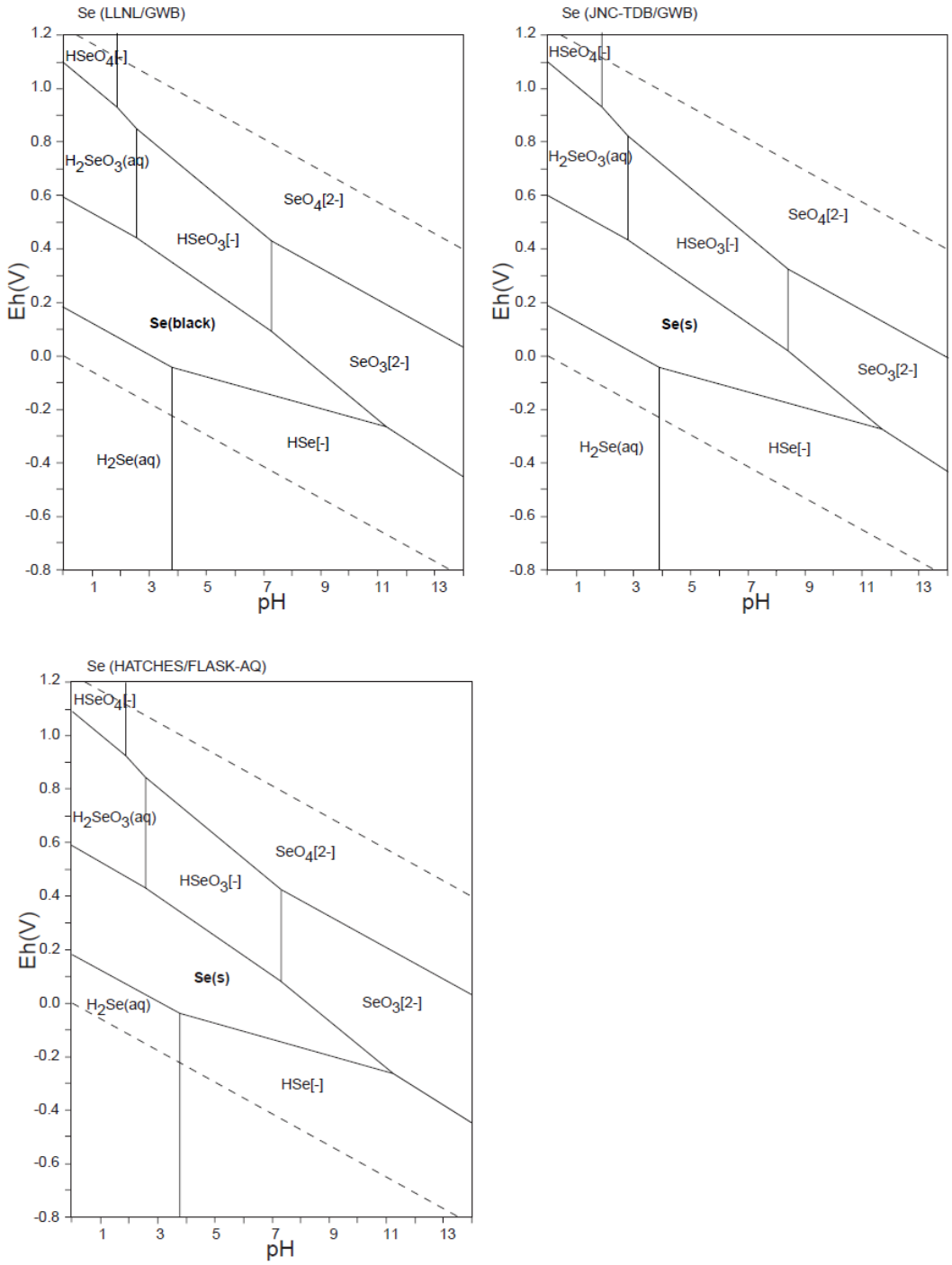

Figure 3-1: The Pourbaix diagrams of selenium according to FACT database, SUPCRT database, LLNL database, JNC-TDB database and HATCHES database. [56].

The solubility of selenium is dependent on redox conditions. Under oxidizing conditions, Se(IV) and Se(VI) salts are very soluble and mobile.

Under slightly reducing Boom Clay conditions (-450 mV < Eh <-250 mV, pH~8.5), all databases agree that under such conditions hydroselenide (HSe^-) should be the stable

specie. However according to De Cannière et al. [57], the mobility of HSe^- migration is limited by the solubility of poorly soluble compounds of Se(0) and iron selenide.

On the other hand, in practical terms, due to uncertainty and difficulty of chemical reduction of selenium in higher oxidation states in the absence of catalyst in Boom Clay conditions, most selenium present in radioactive waste (spent fuel or vitrified waste) is proven to be in the form of soluble selenite (SeO_3^{2-}) or selenate (SeO_4^{2-}) ions. Hence, investigation of selenite or selenate migration in Boom Clay is the focus at present.

3.2 Selenium interaction with bentonite

Sorption onto bentonite will play an important role in retarding nuclide migration in geosphere. Various researchers have reported that anions diffuse through the free pore space and cations diffuse through the interlayer space of bentonite.

Boult et al. [58] investigated Se(IV) interaction with purified Na-bentonite, as well as goethite and smectite which are both important compounds of bentonite. For purified bentonite, Se(IV) was proven significantly adsorbed only below pH 7. As for goethite, strong sorption of Se(IV) was observed below pH 8, while for smectite sorption was only significant at low pH level. Surface complexation was considered the most likely mechanism for Se(IV) sorption onto purified bentonite and goethite.

Sato and Miyamoto [59] determined apparent diffusivities for selenite (SeO_3^{2-}) and hydroselenide (HSe^-) in compacted bentonite in presence of silicates at 22.5 and 60°C. Under reducing conditions, apparent diffusion coefficient of HSe^- obtained is 1 order of magnitude lower than that of SeO_3^{2-}. Silicate content, temperature and smectite content were all proven to affect selenium migration in compacted bentonite.

Wu et al. [60] investigated the effect of salt concentration, in this case 0.05 to 1.0 mol/L $NaClO_4$, on migration of Re(VII) and Se(IV) in bentonite by through-diffusion experiments. They highlighted that there was no significant influence of elevated ionic strength on adsorption of Se(IV) in Gaomiaozi (GMZ) bentonite, but an increasing of effective diffusion coefficient, indicating inner-sphere surface complexions.

Another technique designed to enable accelerated migration experiments is electromigration. Experiments using electromigration technique investigating selenium migration in bentonite were conducted by Maes et al. [61, 62], Beauwens et al. [63], Bruggeman et al. [64], De Cannière et al. [57], and Zappey, Carter and Vermunt in our group [65-67].

3.3 Selenium interaction with Boom Clay

In aqueous solutions, SeO_4^{2-}, SeO_3^{2-} and HSe^- as forms of selenium are present. Under conditions of Boom Clay, only selenite (SeO_3^{2-}) forms inner-sphere complexes that are

stable at neutral and slightly alkaline pH and can sorb on oxide surfaces by surface complexation reactions. With selenate (SeO_4^{2-}), outer-sphere complexes are formed under Boom Clay conditions. Hence, sorption of selenate is weaker than selenite and requires low pH conditions [57].

The spectroscopic data are adequate to provide information about the selenium environment under Boom Clay conditions. Bruggeman [68] conducted XANES and EXAFS measurements on illite du Puy in contact with selenite solution. Spectra of XANES and EXAFS measurements reflected the existence of the $HSeO_3^-$ species. By Fourier-transformed radial structure function (RSF) of EXAFS spectra, formation of inner-sphere complexions of selenite on clay platelet edges was proven.

In Boom Clay, no sorption has been observed in batch tests for selenate (SeO_4^{2-}) which is not known to form strong inner-sphere complexes with hydroxylated surfaces at in situ pH value representative of Boom Clay. According to results of investigation conducted by De Canniere et al. [57], selenate is very weakly or not adsorbed and reduced under reducing conditions in Boom Clay. Meanwhile, selenate was proven not solubility limited and not associable with organic matters.

Table 3-1: Interactions expected for inorganic Se species in Boom Clay [57].

Oxidation State	Species	Sorption	Reduction	Precipitation	OM Association
+6	$SeO_4^{2-}{}_{(aq)}$	Very low	Extremely reluctant	No solubility limit	None
+4	$SeO_3^{2-}{}_{(aq)}$	Medium (inner-sphere complex)	Easy	$CaSeO_3$ (+ solid solution in cement)	Association (+ reduction) observed
0	$Se_{(s)}$	—	Slow	Se	Colloid – colloid
–2	$HSe^-{}_{(aq)}$	Unknown (not considered)	—	$FeSe_2$, Fe_xSe_y	None

Electromigration experiments investigating selenium migration in Boom Clay were conducted by Beauwens et al. [57, 63]. Due to short time span of the experiments, more experiments with various parameters are required in order to obtain reliable results along with the existent data.

4 Overview of migration experiments

Several types of migration experiments are available to determine the migration parameters of radionuclides in the clay. Two types of experiments exist: (a) pure diffusion experiments, with merely a concentration gradient, and (b) dispersion/advection experiments with an additional hydraulic pressure besides the concentration gradient [64].

4.1 Pure diffusion experiments

Two types of pure diffusion experiments are usually adopted in scientific research, i.e. through-diffusion experiments and in-diffusion experiments (Figure 4-1).

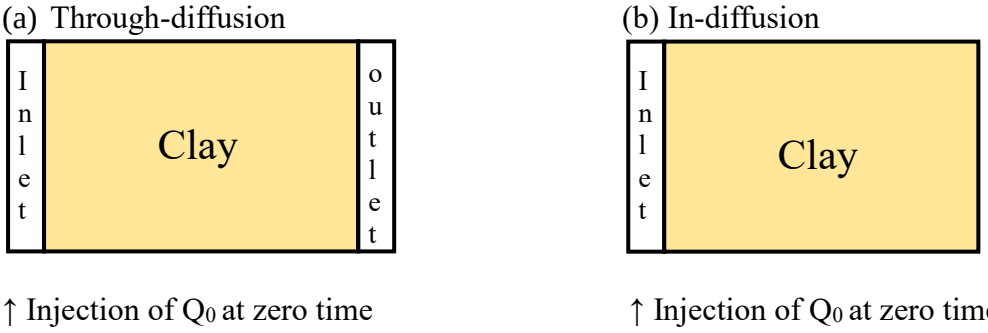

Figure 4-1: Schematic figures of through-diffusion (a) and in-diffusion (b) experiments.

In through-diffusion experiments, the clay core is confined between two well-stirred solution compartments (Figure 4-1a). The tracer element is initially added to the inlet compartment and diffuses towards the outlet through clay core. Content of the tracer element in the outlet compartment is measured as a function of time. If throughout the experiment no tracer is detected in the outlet compartment, a through-diffusion experiment could be considered as an in-diffusion one.

In-diffusion experiments are very much similar to the through-diffusion experiments (Figure 4-1b). However, in the given period of time of in-diffusion experiments, tracer elements are not able to reach the end of the clay core. Content of tracer elements at different depths of clay core are measured in in-diffusion experiments.

4.2 Dispersion/advection experiments

Dispersion/advection experiments allow simultaneous determination of the hydraulic conductivity as well as the migration parameters of the tracer in the clay core.

Two types of dispersion/advection experiments are usually adopted in scientific

research, i.e. percolation experiments (Figure 4-2a) and pulse injection experiments (Figure 4-2b).

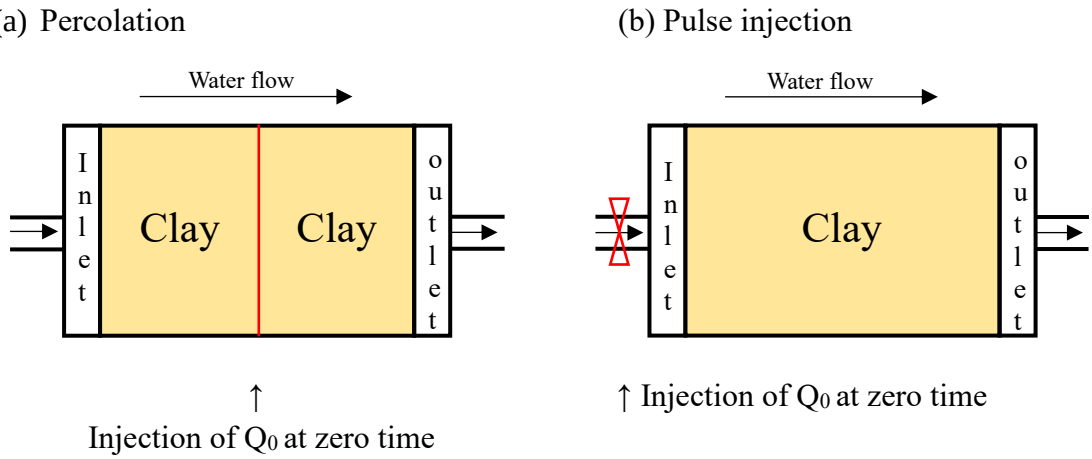

Figure 4-2: Schematic figures of percolation and pulse injection experiments.

The simplest set-up of dispersion/advection experiments is percolation. In percolation experiments, tracer elements are spiked in the middle of two clay core that connected to each other, while the clay cores are then confined between two filters. The water flowing out of the system is collected at the outlet and the content of tracer elements in the water are measured as a function of time.

Pulse injection experiments are similar to the percolation experiments. However, rather than have two clay cores, in set-up of pulse injection experiments only one clay core is confined between two filters, and the tracer is spiked at the inlet rather than in the middle. Same as the percolation experiments, the water flowing out of the system is collected at the outlet and the content of tracer elements in the water are measured as a function of time.

4.3 Electromigration experiments

Above mentioned types of migration experiments have a common disadvantage of long experimental time. Though exerted hydraulic pressure could accelerate the migration of radionuclides to a certain extent, a quite high hydraulic pressure is usually required due to the relatively low hydraulic conductivity of clay.

To accelerate the process of migration, applying an electric field would be a more sophisticated approach. Small electric field exerted can easily enhance the migration process to an extent that is extremely difficult to be reached by applying hydraulic pressure.

In spite of high efficiency to accelerate experiments, disadvantages such as electrolysis of water during electromigration should be taken into account. Due to the potential

difference between cathode and anode, water is decomposed into hydrogen and oxygen respectively at cathode and anode. Corresponding electrode reactions are:

Cathode (reduction)

$$2H^+ + 2e^- \rightarrow H_2(\uparrow) \quad \text{(Eq. 4.1)}$$

Anode (oxidation)

$$2OH^- - 2e^- \rightarrow H_2O + \frac{1}{2}O_2(\uparrow) \quad \text{(Eq. 4.2)}$$

Thus, the overall reaction of electrolysis is:

$$H_2O \xrightarrow{electrolysis} H_2(\uparrow) + \frac{1}{2}O_2(\uparrow) \quad \text{(Eq. 4.3)}$$

To keep the experimental results accurate and reliable from local acidification and alkalization at the compartments, liquid from the two compartments is continuously transferred to and mixed in an external reservoir and transferred back by peristaltic pumps during experiments.

5 Governing transport equation

5.1 Mass transport of ionic species

To describe the migration process of radioactive nuclides under the effect of electric field in a clay material, a one-dimensional convection–dispersion equation is usually adopted, which is in the form of:

$$\frac{\partial C}{\partial t} = \nabla \cdot (D \nabla C) - \nabla (V_c \cdot C) \quad \text{(Eq. 5.1)}$$

where C is the specie concentration, D is the dispersion coefficient, V_c is the average convection velocity. The first term on the right-hand side of equation represents dispersion driven by concentration gradient and mechanical dispersion and the second term represents convection, including electromigration and electroosmosis.

With the existence of applied electric field, the electrokinetic process can usually be divided into two parts: electromigration (V_{em}) and electroosmosis (V_{eo}). The velocities of these two processes make up the average convection velocity, namely:

$$V_c = V_{em} + V_{eo} \quad \text{(Eq. 5.2)}$$

Electromigration is the transport of ions through the material towards the electrode of opposite sign, namely cations towards cathode (-), anions towards anode (+). The velocity of this process is proportional to the electric field applied:

$$V_{em} = \mu_{em} \cdot E \quad \text{(Eq. 5.3)}$$

where μ_{em} is the ionic mobility in electromigration, E is the electric field applied.

Electroosmosis is the other process in electrokinetic processes. With an electric field applied, the counter ions (cations) near the negatively charged clay mineral surface tend to migrate towards the electrode of opposite sign, namely cathode. Since many of the counter ions are solvated, especially in diffuse layer of double electric layer, a drag force is exerted on water molecules to migrate together with counter ions to cathode. The velocity of this process is as well proportional to the electric field applied:

$$V_{om} = \mu_{om} \cdot E \quad \text{(Eq. 5.4)}$$

where μ_{om} is the ionic mobility in electroosmosis, E is the electric field applied.

Due to the difference in migration directions between cations and anions, in electromigration and electroosmosis, the average convection velocity V_c can have different values for cations and anions. The effect by this difference will be discussed in the following part.

For a real porous clay material, the general form of convection-dispersion equation should be corrected by retardation effects and tortuosity. Based on the assumption of a linear sorption isotherm, the retardation factor R can be expressed as:

$$R = 1 + \frac{\rho_d}{\eta_{diff}} \cdot K_d \quad \text{(Eq. 5.5)}$$

where ρ_d is the dry density, K_d is the distribution coefficient and η_{diff} is the diffusion accessible porosity.

The simplest mathematical definition of tortuosity is the arc-chord ratio, namely the ratio of the length of the curve to the distance between the ends of it:

$$\tau = \frac{C}{L} \quad \text{(Eq. 5.6)}$$

Thus, the corrected convection-dispersion equation is:

$$R \cdot \frac{\partial C}{\partial t} = \nabla \cdot (D \nabla C) - \nabla (V_c' \cdot C) = D \cdot \frac{\partial^2 C}{\partial x^2} - \frac{V_c}{\tau} \cdot \frac{\partial C}{\partial x} = \frac{D}{\tau^2} \cdot \frac{\partial^2 C}{\partial z^2} - \frac{V_c}{\tau} \cdot \frac{1}{\tau} \cdot \frac{\partial C}{\partial z}$$

i.e.:

$$\frac{\partial C}{\partial t} = \frac{D}{R \cdot \tau^2} \cdot \frac{\partial^2 C}{\partial z^2} - \frac{V_c}{R \cdot \tau^2} \cdot \frac{\partial C}{\partial z} \quad \text{(Eq. 5.7)}$$

where x is the migration distance at microscopic scale and z is the migration distance at macroscopic scale.

The terms of $D/(R \cdot \tau^2)$ and $V_c/(R \cdot \tau^2)$ are then defined as the apparent dispersion coefficient D^a and the apparent convection velocity V_c^a. As a result, the convection-dispersion equation is back to its general form:

$$\frac{\partial C}{\partial t} = D^a \cdot \frac{\partial^2 C}{\partial z^2} - V_c^a \cdot \frac{\partial C}{\partial z} \quad \text{(Eq. 5.8)}$$

A solution of Eq. 5.8 with appropriate boundary conditions introduced is given below [21][22]:

$$C(x, t) = \frac{Q_0}{2S\sqrt{\pi D^a t}} \cdot \exp\left(-\frac{(x - V_c^a t)^2}{4 D^a t}\right) \quad \text{(Eq. 5.9)}$$

where Q_0 is the initial activity spiked at the source position and S is the cross-section area of clay plug.

Boundary conditions introduced [22]:

$$C(x = \infty, t = 0) = 0$$
$$C(x = \infty, 0 < t < \infty) = 0$$
$$C(0 < x < \infty, t = 0) = 0$$

5.2 Derivation of the apparent diffusion coefficient

5.2.1 Method 1: hydrodynamic dispersion relation

When advective migration increase relatively compared with diffusive transport, not only diffusion but also hydrodynamic dispersion occurs [23]. This can be described in the relation:

$$D^a = D_m^a + \alpha V_c^a \quad \text{(Eq. 5.10)}$$

where D_m^a is the apparent diffusion coefficient and α is the dispersion length, which is a characteristic of porous materials.

By fitting the measured distribution profiles with Eq. 5.9, a series of D^a values and V_c^a values will be obtained from the calculation in Matlab. Hence, by plotting apparent dispersion coefficient D^a as a function of apparent convection velocity V_c^a with a series of data points from calculation, the dispersion length α as the slope and the apparent diffusion coefficient D_m^a as the intercept of the regression line are obtained.

5.2.2 Method 2: Nernst–Einstein relation

Similar with Eq. 5.3 and Eq. 5.4, the apparent convection velocity can also be expressed as:

$$V_c^a = \mu^a \cdot E \quad \text{(Eq. 5.11)}$$

where μ^a is the apparent ionic mobility.

As mentioned above, due to the difference in migration directions between cations and anions, in electromigration and electroosmosis, the average convection velocity V_c can have different values for cations and anions.

For cations,

$$\mu^a = \mu_{em}^a + \mu_{om}^a = \frac{\mu_{em}+\mu_{om}}{R\cdot\tau^2} \quad \text{(Eq. 5.12)}$$

For anions,

$$\mu^a = \mu_{em}^a - \mu_{om}^a = \frac{\mu_{em}-\mu_{om}}{R\cdot\tau^2} \quad \text{(Eq. 5.13)}$$

According to the Nernst-Einstein equation, the diffusion coefficient of ionic species in free water D_0 can be expressed as a function of the ionic mobility μ_{em}:

$$D_0 = \mu_{em} \cdot \frac{kT}{Ze} \quad \text{(Eq. 5.14)}$$

To investigate porous materials like clay materials, corrections of sorption, tortuosity and electroosmosis are necessary. Thus:

$$D_m^a = \mu^a \cdot \frac{kT}{Ze} = (\mu_{em}^a \pm \mu_{om}^a) \cdot \frac{kT}{Ze} = \frac{D_0}{R\cdot\tau^2} \pm (\mu_{em}^a \cdot \frac{kT}{Ze}) \quad \text{(Eq. 5.15)}$$

Through a series of experiments with varying electric field applied, the apparent ionic mobility of electroosmosis process μ_{om}^a can be obtained from the slope of Eq. 5.16.

$$V_c^a = \mu^a \cdot E = (\mu_{em}^a \pm \mu_{om}^a) \cdot E \quad \text{(Eq. 5.16)}$$

Then, with known value of μ_{em}^a, the apparent diffusion coefficient is able to be

calculated with Eq. 5.15.

6 Materials and methods

6.1 Clay chemical and structural characterization

In addition to migration experiments for determining the diffusion coefficient of the buffer material or clay host rock, the chemical stability of the multi-barrier structure over long-term service is also vital to the competence.

The original chemical composition of Boom Clay and original porosity were characterized to make it possible to examine what change and to what extent the interactions between the barrier materials can bring to the structure. The relevant parameters after interface interactions would be as well characterized in future researches. The techniques related are, instrumental neutron activation analysis (INAA) for accurate chemical composition measurements and mercury intrusion porosimetry (MIP) for characterization for material pore structure.

6.1.1 Instrumental neutron activation analysis

Instrumental neutron activation analysis (INAA) is a highly sensitive technique that can make qualitative and quantitative analysis on elemental composition of materials.

In a neutron activation analysis, the sample material is irradiated with neutrons in a nuclear reactor. During this process, some stable isotopes are converted into corresponding radioactive isotopes. Along with isotopes decaying over time, gamma radiation with various characteristic energies are emitted. By measuring the intensity of such characteristic energies, the concentrations of corresponding elements are obtained. Due to the high sensitivity, only small amount of sample material, around 100 to 200 mg, is sufficient for the analysis. On the other hand, due to the mechanism this type of analysis is based on, elements that do not yield gamma-ray emitting radionuclides cannot be detected by INAA. Additionally, a long duration of analysis is possibly required depending on the type of elements because some form relatively long-lived nuclides.

The results obtained from this analysis are unbiased element concentrations, without detection limits or upper limits in them. Consequently, all data have the same physical meaning and can be interpreted in a straightforward statistical sense.

6.1.2 Mercury intrusion porosimetry

Mercury is the only kind of liquid-state metal at ambient condition. It is not able to wet most substances and hence not able to penetrate pores by capillary action, unless a sufficient external pressure is exerted. According to parameters including surface tension γ and wetting angle θ, a circular pore with a pore size of D has a resisting force

to penetration:

$$f_R = \pi D \gamma cos\theta \quad \text{(Eq. 6.1)}$$

Assuming a pressure is exerted to overcome such resistance, hence:

$$f_{Ext} = pA = {}^{p\pi D^2}/_{4} \quad \text{(Eq. 6.2)}$$

According to force equilibrium, we can derive:

$$-\pi D \gamma cos\theta = {}^{p\pi D^2}/_{4} \quad \text{(Eq. 6.3)}$$

Hence:

$$p = -4\gamma cos\theta / D \quad \text{(Eq. 6.4)}$$

Thus, a conclusion can be drawn that the pressure needed to facilitate penetration of mercury into pores with a certain pore size is inversely proportional to the pore size. In mercury intrusion porosimetry measurements, mercury is continuously pressed into the material characterized with a gradually increasing pressure. Volume of mercury intruded into materials is recorded at each pressure level, which corresponds to a specific pore size. Eventually, a profile of volume occupied by different sizes of pores can be drawn.

6.2 Bentonite-characterization of starting material

Bentonite used in this project is commercial bentonite MX-80 powder mined in Wyoming, USA. Technique of X-ray fluorescence (XRF) was used to characterize the elemental composition of bentonite raw material. The elemental composition is given below.

Table 6-1: Elemental composition of bentonite (MX-80).

Element	Compound	Content (wt%)
Si	SiO_2	63.32
Al	Al_2O_3	19.96
Ca	CaO	2.89
Na	Na_2O	3.26
Mg	MgO	3.00
Fe	Fe_2O_3	5.04
K	K_2O	0.67
Cr	Cr_2O_3	0.02
Mn	MnO	0.04
Ti	TiO_2	0.66
Ba	BaO	0.08
Zn	ZnO	<0.02

Pb	PbO	<0.02

From the results of XRF measurements, it can be seen that bentonite is mostly composed of elements Si and Al, while small amount of other metal elements including Ca, Na, Mg and Fe exist as well.

This elemental composition obtained has a good agreement with the phase composition of bentonite reported by Karnland [30], according to whom bentonite was basically composed of montmorillonite. The average composition of montmorillonite was reported to be $(Na,Ca)_{0.33}(Al,Mg)_2(Si_4O_{10})(OH)_2 \cdot nH_2O$.

The clay plaster is then filled into two cylindrical polycarbonate tubes. The polycarbonate tubes are each 5 cm in length and 3 cm in diameter. Then the tubes were aligned, fitted into electromigration cell and sealed with two porous ceramic filters at the outmost ends. The porous ceramic filters have a diameter of 40 mm and a pore size of 10 to 16 μm, allowing solution flowing through but preventing penetration of clay particles.

6.3 Boom Clay-characterization of starting material

Boom Clay used in this project was drilled from ~80 m depth from Zeeland region in the Netherlands. According to Arnold et al. [69], the Belgian Boom Clay is a homogenous sediment with a varied mineralogy mostly composed by clay minerals (Kaolinite, Smectite and Illite) and non-clay minerals (Quartz, K-feldspar, Na-plagioclase and Carbonates). A complete mineralogical characterization of the Dutch Boom clay drilled from various regions was presented by Koenen et al [28]. The samples consisted mainly of quartz (16.3-86.3 wt%) and clay minerals (8.4-70.2 wt%, from bulk analysis). Plagioclase and K-feldspar were present in all samples and varied between 0.3-5.6 and 2.2-11.1 wt% respectively. The carbonate content varied strongly between the samples and consisted of calcite (up to 25.9 wt%), aragonite (up to 5.1 wt%) and occasionally small amounts of ankerite/dolomite and siderite. Pyrite and anatase were present in almost all samples with values up to 6.9 and 0.9 wt% respectively.

A mineralogical characterization of the Dutch Boom Clay was performed in order to identify the existent phases. Characterization was performed by X-ray diffraction (XRD) onto crushed clay and revealed the existence of quartz, pyrite and muscovite as main crystalline phases.

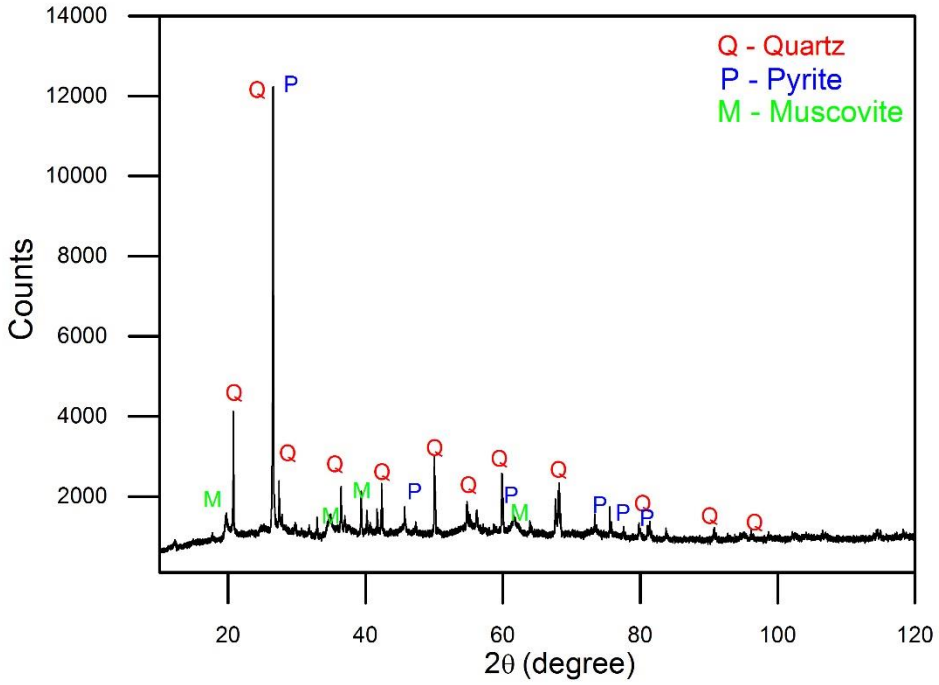

Figure 6-1: XRD pattern of crushed Boom Clay sample.

By X-ray fluorescence (XRF), the mean elemental composition of the Boom Clay was characterized and displayed in Table 6-2. The main components are Si, Al and Fe, with existence of K, Ca and Mg in small amounts. These results generally agree with the researches by Volckaert [34], Van Keer [37] and De Craen [36] while the content of Fe element is relatively higher, indicating a higher content of pyrite in Boom Clay investigated.

Table 6-2: Elemental composition of Boom Clay.

SiO_2	Al_2O_3	Fe_2O_3	K_2O	CaO	MgO
60.34	17.64	8.9	2.8	1.16	2.31

Microstructure of Boom Clay was examined by scanning electron microscope. In addition to the amorphous matrix, a large quantity of conglobate spherulites was observed and afterwards proven to be pyrite crystals by Energy Dispersive Spectrometer (EDS).

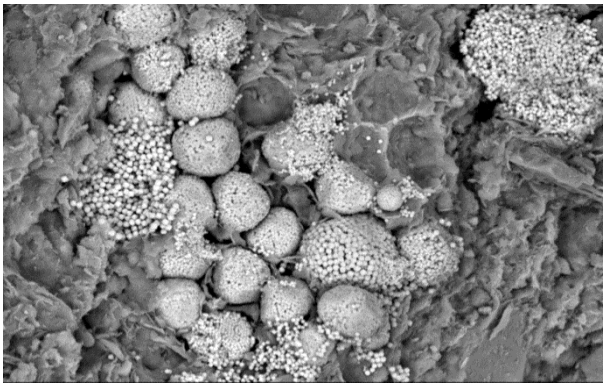

Figure 6-2: SEM image of surface of Boom Clay sample.

6.4 Clay cores preparation

6.4.1 Bentonite cores

To prepare clay cores for electromigration experiments, bentonite powder was mixed with water according to a certain proportion and made into wet plaster. The plaster was kneaded thoroughly, making the samples homogeneous, and then filled into two cylindrical polycarbonate tubes. The polycarbonate tubes are each 5 cm in length and 3 cm in diameter. Then the tubes were aligned, fitted into electromigration cell and sealed with two porous ceramic filters at the outmost ends. The porous ceramic filters have a diameter of 40mm and a pore size of 10 to 16 μm, allowing solution flowing through but preventing penetration of clay particles.

After clay cores been prepared, the electrolyte solution was then prepared. In this project, 15 mM $NaHCO_3$ solution is chosen as the clay pore water in experiments investigating the inherent diffusion coefficient of selenate ion in bentonite; a solution consisting of 15 mM $NaHCO_3$ and 1 mM H_4SiO_4 is chosen in experiments investigating the effect of silicic acid existence can cause to the diffusion coefficient of selenate ion in bentonite; and a detailed recipe of Boom Clay pore water is adopted based on a series of assumptions on the Dutch marine environment and Boom Clay composition.

6.4.2 Boom Clay cores

Due to the natural existence of a large amount of microcracks in Boom Clay rock, cutting the clay rock into intact cylinder samples was tricky and unreliable. Hence, in this project, Boom Clay rock was first prepared into clay powder, then made into wet plaster and then finally shaped into the desired shape.

Because of the ubiquitous presence of pyrite (FeS_2), Boom Clay has an oxidation sensitive composition. Oxidation of pyrite can be expressed as:

$$\mathrm{Fe}S_2 + \frac{7}{2}O_2 + H_2O \rightarrow Fe^{2+} + 2SO_4^{2-} + 2H^+ \quad \text{(Eq. 6.5)}$$

The reaction essentially releases acid and sulphate ions. Such reaction can affect geochemical characteristics of the clay, pH level of clay pore water and sorption properties of radionuclides in clay [70, 71]. Porosity of clay, as well as of contacting concrete buffer/backfill, can also be modified by pyrite oxidation, further affecting hydraulic conductivity of clay and thus the transport of radionuclides.

To avoid such interactions with atmosphere as much as possible, storage and preparation process of Boom Clay were all carried out in oxygen-free environments. Before experiments, clay samples were vacuum-packed in aluminium-coated polyethylene bags and store in a glove box filled with argon. Sample preparation process was as well always carried out in anaerobic conditions in a glove box (oxygen level < 10 ppm). The samples were taken out of the aluminium-coated polyethylene bags and made into powder with grinding tools. The clay powder was then mix with Boom Clay pore water in a certain ratio into plaster. The plaster was kneaded thoroughly, making the samples homogeneous, and then filled into two cylindrical polycarbonate tubes. The polycarbonate tubes are each 5 cm in length and 3 cm in diameter. Then the tubes were aligned, fitted into electromigration cell and sealed with two porous ceramic filters at the outmost ends. The porous ceramic filters have a diameter of 40mm and a pore size of 10 to 16 μm, allowing solution flowing through but preventing penetration of clay particles.

In experiments investigating inherent transport properties of Dutch Boom Clay, since the Netherlands has not yet established any repository structure or decided the location of the future site, a porewater composition was especially designed, based on the average conditions of Dutch marine environment by the company COVRA. Detailed composition of both kinds of Boom Clay pore water is introduced in Appendix A.

6.5 Selenium tracer solution preparation

In this project, instead of long lived Se-79, Se-75 with a 120-day half-life was adopted to be the tracer nuclide. 25 mg of SeO_2 was irradiated for 10 hours in the HOR reactor of Reactor Institute Delft to obtain an activity of 0.8 MBq. During irradiation, thermal neutron flux was 4.80×10^{16} $s^{-1}\cdot m^{-2}$, epithermal neutron flux was 7.59×10^{14} $s^{-1}\cdot m^{-2}$ and fast thermal flux was 3.38×10^{15} $s^{-1}\cdot m^{-2}$. The irradiated sample was then cooled for 3 days before collected. The neutron capture reaction occurred during irradiation is:

$$^{74}_{34}Se + ^{1}_{0}n \rightarrow ^{75}_{34}Se + \gamma \quad \text{(Eq. 6.6)}$$

Since SeO_2 is one immobile species in Boom Clay pore water, irradiated SeO_2 sample was then prepared into selenate (SeO_4^{2-}) which is highly mobile in Boom Clay and better suited for transport experiments. Selenate was prepared by oxidizing SeO_2 with 1 mL oxidizing agent hydrogen peroxide (H_2O_2):

$$SeO_2 + H_2O_2 \rightarrow H_2SeO_4$$ (Eq. 6.7)

Migration mechanism of selenium in clay and concrete layers is very much dependent on the valence state and adsorption, oxidation, reduction, precipitation and other processes corresponding to each valence.

6.6 Electromigration

The electromigration cell was design based on the experimental set-up proposed by researchers from Belgian Nuclear Research Centre (SCK·CEN) [61]. A schematic diagram is given below:

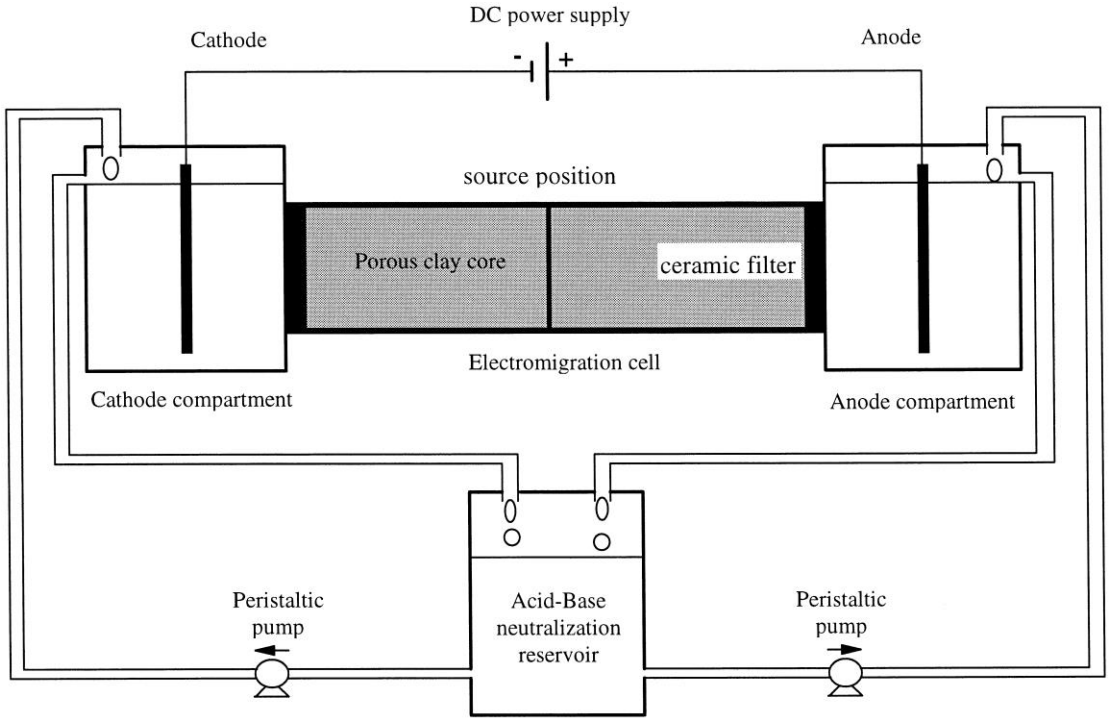

Figure 6-3: Schematic diagram of the electromigration set-up [61].

With clay cores and clay pore water prepared and filled in, the cell was then connected to a power supply in electric circuit. A current of approximately 15 mA is often exerted to facilitate the process. The varying electric field in the clay cores were monitored and recorded by a voltmeter which was connected to ends of the clay cores. The completion of saturation process can be proven by the rough stabilization of electric field measured. Previous work reported that such saturation process usually takes no more than 6 hours.

After saturation, an aqueous path for nuclides migration was well established. Then the radioactive (or nonradioactive) tracer nuclide was spiked in the middle of two clay cores. 50 μL of above mentioned selenate tracer solution was applied, with activity of approximately 40 kBq. To be more specific, the spiking was done by wetting a piece of filter paper with the tracer solution mentioned previously and then sealing the cell completely again.

After that, the electromigration process was carried out with certain current level exerted during the process and for certain length of time. Specific parameters of current and time span were chosen on purpose to obtain a series of well dispersed data points, so that the value of apparent diffusion coefficient can be derived from linear regression.

To balance local acidification and local alkalisation induced by electrode reactions occurring at cathode compartment and anode compartment, the compartment solution at both sides was continuously taken out of the cell by two peristaltic pumps, mixed in a neutralisation reservoir and pumped backed in the same rate. The level of pH was regularly checked during saturation process and electromigration process for safety reasons, as well as overheating or not and leakage or not.

When the electromigration with certain period of time was completed, the clay cores were taken out of the cell and cut into slices with thickness 3 mm. The activity contributed by tracer nuclides in each slice was measured by gamma spectrometer to obtain a distribution profile. Clay slices were transferred into centrifuge vials and mixed with 30 mL water. After being shaken overnight, clay particles were well dispersed in liquid. 10 mL liquid was taken from each piece of suspension liquid made from the slices and transferred into scintillation vials for gamma spectrometer measurements. After 10-minutes measurements for each vial, a distribution profile of activity contributed by tracer nuclides was drawn. Further by calculations and fitting in Matlab, the dispersion coefficient D_i and the apparent convective velocity V^a were obtained, based on Eq. 5.9 mentioned previously. By linear regression of D_i-V^a diagram, the apparent diffusion coefficient, which is the ultimate aim of the electromigration experiments, was obtained.

7 Results and discussion

7.1 Electromigration experiments

7.1.1 Electromigration experiments performed on bentonite

In the electromigration experiments conducted on bentonite, the inherent diffusion coefficient of selenate ion (SeO_4^{2-}) in bentonite and the effect of silicic acid on the diffusion coefficient were investigated.

A series of experiments were conducted, in which the current exerted during electromigration and the duration were the variables. The currents exerted were in a range of 5 to 20 mA and the duration in a range of 7 to 48 hours. The parameters adopted were designed based on a balance between maximizing varying ranges to obtain sufficient and reliable results and keeping parameters within safe limits.

For each electromigration experiment, a distribution profile was drawn with the concentrations of selenate tracer ion (SeO_4^{2-}) at different depths of clay core. The peak location of the profile and the peak width were respectively determined by the corresponding apparent convection velocity and the dispersion coefficient. The distribution profiles of selenium concentration in bentonite after electromigration without silicate existence were displayed in Figure 7-1. A general rule can be observed from the profiles, that current applied and duration of time together decided the location of peak and longer time led to larger dispersion.

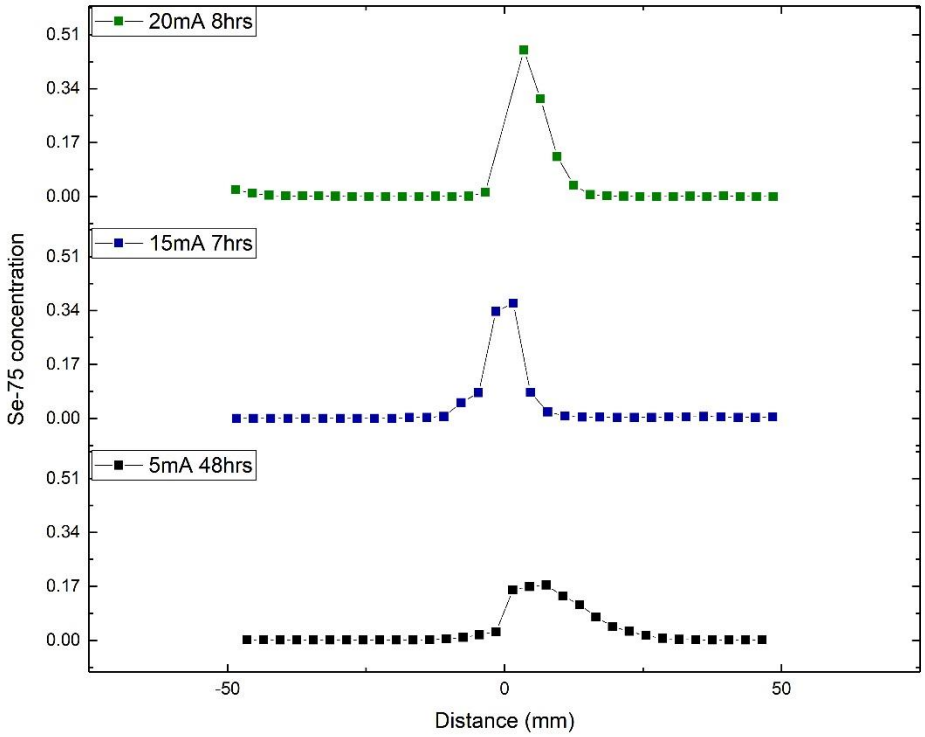

Figure 7-1: The distribution profiles of selenium concentration in bentonite after electromigration without silicate existence.

Method 1: hydrodynamic dispersion relation

By function fitting of the distribution profile with Eq. 5.9, apparent convection velocity and dispersion coefficient were calculated. The calculated apparent convection velocities and dispersion coefficients from the results of electromigration with bentonite (without existence of silicic acid) are summarized in the Table 7-1 below. And a comparison with the results from Vermunt [65] from our group is given in Table 7-2.

Table 7-1: Apparent convection velocities and dispersion coefficients calculated from the results of electromigration with bentonite.

Apparent velocity m/s	**Dispersion coefficient m^2/s**	**Current mA**	**Electric field V/m**	**Duration hrs**
4.34E-08	1.28E-10	5	77.33	48
6.20E-08	3.08E-10	15	110.67	7
1.50E-07	2.66E-10	20	389.33	8

Table 7-2: Comparison of results with predecessor Vermunt [65].

Apparent velocity (m/s)	Dispersion coefficient (m^2/s)	Current (mA)	Duration (hrs)
4.34E-08	1.28E-10	5	48
6.20E-08	3.08E-10	15	7
1.24E-07	2.16E-10	12	19
1.50E-07	2.66E-10	20	8
1.74E-07	5.12E-10	10	8
1.98E-07	5.50E-10	15	7

With such series of apparent velocities and dispersion coefficients, the apparent diffusion coefficient of selenate ion can then be obtained through linear regression according to Eq. 5.10.

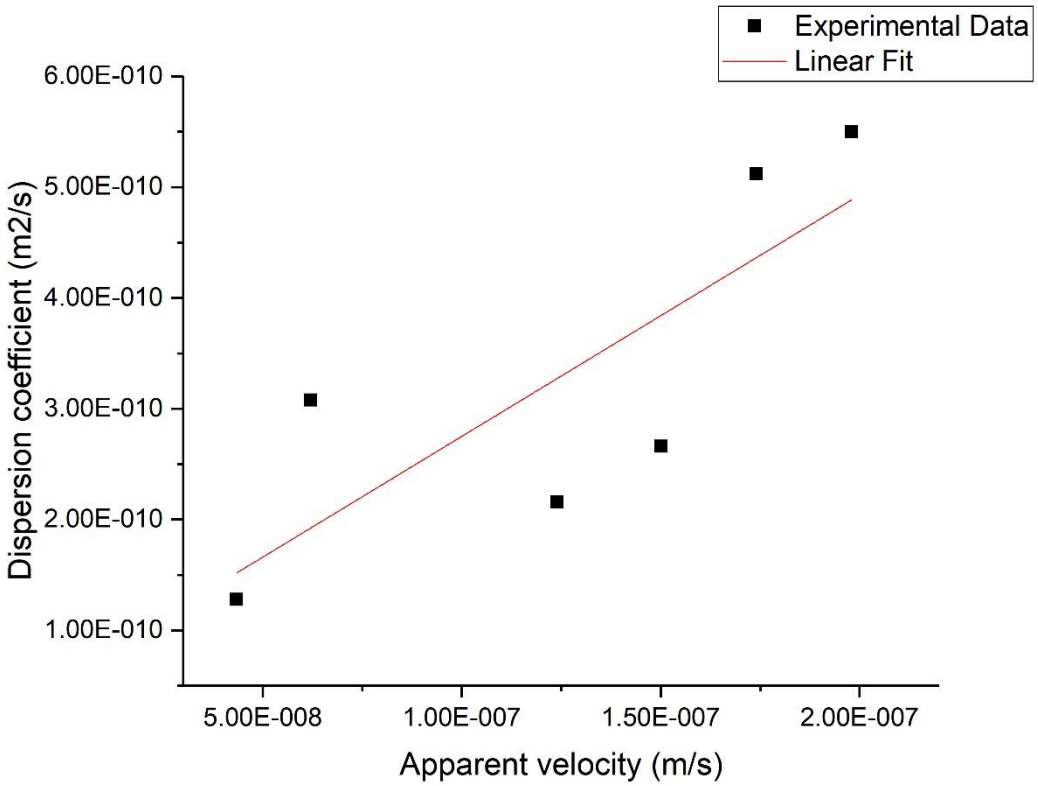

Figure 7-2: Determination of apparent diffusion coefficient of selenate ion in bentonite by linear regression.

From the intercept on y-axis, the apparent diffusion coefficient of selenate ion in bentonite was derived to be 5.71×10^{-11} m^2/s.

Method 2: Nernst–Einstein relation

According to Eq. 5.15,

$$D_m^a = \mu^a \cdot \frac{kT}{Ze} = (\mu_{em}^a \pm \mu_{om}^a) \cdot \frac{kT}{Ze} = (\mu_{em}^a \pm \frac{\mu_{om}}{R \cdot \tau^2}) \cdot \frac{kT}{Ze} \quad \text{(Eq. 7.1)}$$

As for selenate ions as anodic species,

$$D_m^a = (\mu_{em}^a - \frac{\mu_{om}}{R \cdot \tau^2}) \cdot \frac{kT}{Ze} \quad \text{(Eq. 7.2)}$$

The term μ_{em}^a in the equation can be obtained from the slope of apparent convective velovity V_{app} plotting against electric field exerted E according to Eq. 5.3: $V_{em} = \mu_{em} \cdot E$.

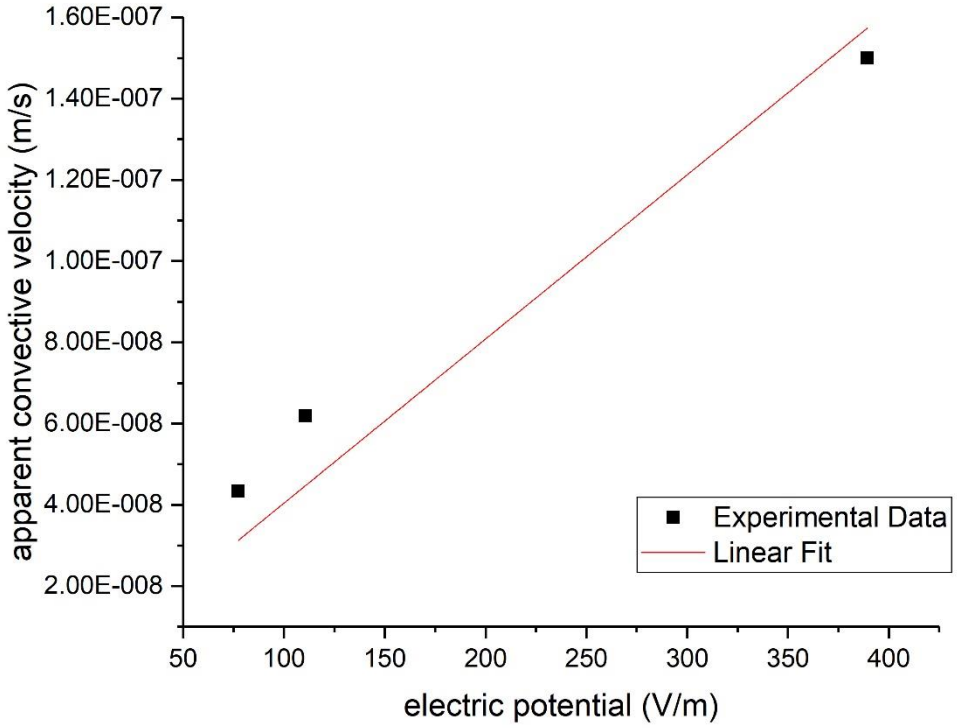

Figure 7-3: Determination of electromigration mobility of selenate ion in bentonite without existence of silicic acid by linear regression.

From linear regression, the μ_{em}^a was determined to be 4.04×10^{-10} $m^2/(V \cdot s)$. Then by Eq. 7.2, the apparent diffusion coefficient of selenate in bentonite can be calculated, as long as the term $\mu_{om}/(R \cdot \tau^2)$ is characterized. Such measurement can be done in electromigration experiments with HTO in bentonite at different electric fields [61]. When the apparent electroosmotic mobility is determined, a comparison of apparent diffusion coefficients obtained by hydrodynamic dispersion relation and Nernst–Einstein relation can be made.

Except the investigations conducted by Zappey [67] at this institute, seldom has ever looked into the migration of selenate ion in bentonite. In most researches carried out with bentonite, selenite ion migration is studied.

According to Zappey, selenate ion in bentonite had an apparent diffusion coefficient of 1.00×10^{-10} m^2/s. Different preparation procedures were adopted in this project and in that of Zappey, denser and more saturated clay samples were prepared in this project thus leading to a relatively lower permeability. Hence, the results generally agree with each other while certain degree of divergence is caused by different preparation processes.

Investigations carried out studying migration of selenite ion indicated an apparent diffusion coefficient in the range of 1.00×10^{-13}-5.00×10^{-10} m^2/s. Idemitsu et al. [72] reported an apparent diffusion coefficient of selenite ion in Kunipia-F bentonite in the range of $(0.19\text{-}25.0)\times10^{-12}$ m^2/s at compacted dry densities of 0.8-1.6 g/cm^3. Sato et al. [73] measured a value of $(3.2\text{-}46)\times10^{-11}$ m^2/s at compacted dry densities of 0.4-1.8 g/cm^3 at pH 9.0 in Na-bentonite. However, no research has yet carried out comparing diffusion coefficients of selenite ion and selenate ion in the same argillaceous rock although difference in sorption kinetics has been widely investigated [51, 52, 74].

It was also reported by some researchers that migration or adsorption of sulphate ion resembled to migration or adsorption of selenate ion on metal oxide surface [57, 75]. Yet seldom investigation has been conducted on sulphate behaviour in bentonite as well.

With existence of silicic acid, a series of experiments were conducted, in which the current exerted during electromigration and the duration were the variables. The currents exerted were in a range of 10 to 30 mA and the duration in a range of 6 to 48 hours. The parameters adopted were designed based on a balance between maximizing varying ranges to obtain sufficient and reliable results and keeping parameters within safe limits.

For each electromigration experiment, a distribution profile was drawn with the concentrations of selenate tracer ion (SeO_4^{2-}) at different depths of clay core. The peak location of the profile and the peak width were respectively determined by the corresponding apparent convection velocity and the dispersion coefficient. The distribution profiles of selenium concentration in bentonite after electromigration with silicate existence are displayed in Figure 7-4. A general rule can be observed from the profiles, that current applied and duration of time together decided the location of peak and longer time led to larger dispersion.

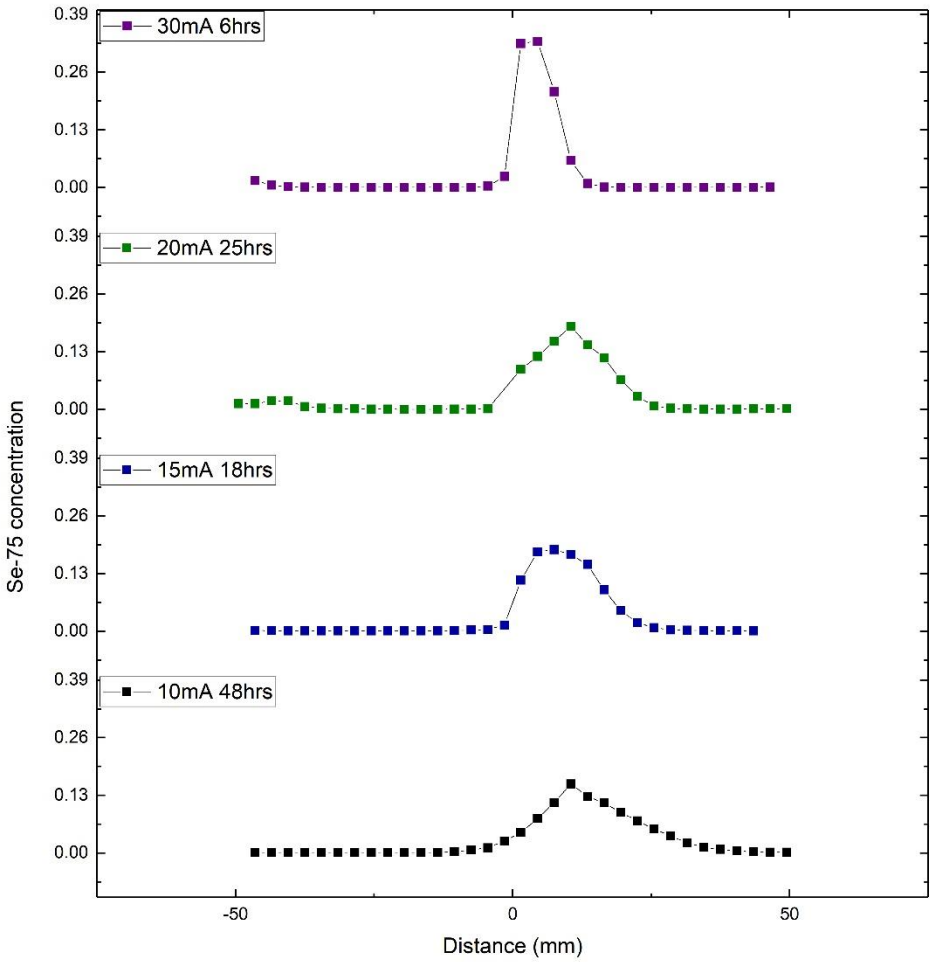

Figure 7-4: The distribution profiles of selenium concentration in bentonite after electromigration with silicate existence.

Method 1: hydrodynamic dispersion relation

By function fitting of the distribution profile with Eq. 5.9, apparent convection velocity and dispersion coefficient were calculated. The calculated apparent convection velocities and dispersion coefficients from the results of electromigration with bentonite (with existence of silicic acid) are summarized in the Table 7-3 below. And a comparison with the results from Vermunt [65] from our group is given in Table 7-4.

Table 7-3: Apparent convection velocities and dispersion coefficients calculated from the results of electromigration with bentonite (with existence of silicic acid).

Apparent velocity m/s	**Dispersion coefficient m^2/s**	**Current mA**	**Electric field V/m**	**Duration hrs**

6.08E-08	2.15E-10	10	126.67	48
1.16E-07	2.85E-10	15	417.33	18
1.17E-07	2.65E-10	20	462.67	25
2.08E-07	2.53E-10	30	1160.00	6

Table 7-4: Comparison of results with predecessor Vermunt [65].

Apparent velocity (m/s)	**Dispersion coefficient (m^2/s)**	**Current (mA)**	**Duration (hrs)**
6.08E-08	2.15E-10	10	48
1.16E-07	2.85E-10	15	18
1.17E-07	2.65E-10	20	25
1.32E-07	3.73E-10	12	21
1.39E-07	4.97E-10	10	8
1.50E-07	8.14E-10	20	6.5
2.08E-07	2.53E-10	30	6

With such series of apparent velocities and dispersion coefficients, the apparent diffusion coefficient of selenate ion can then be obtained through linear regression according to Eq. 5.10.

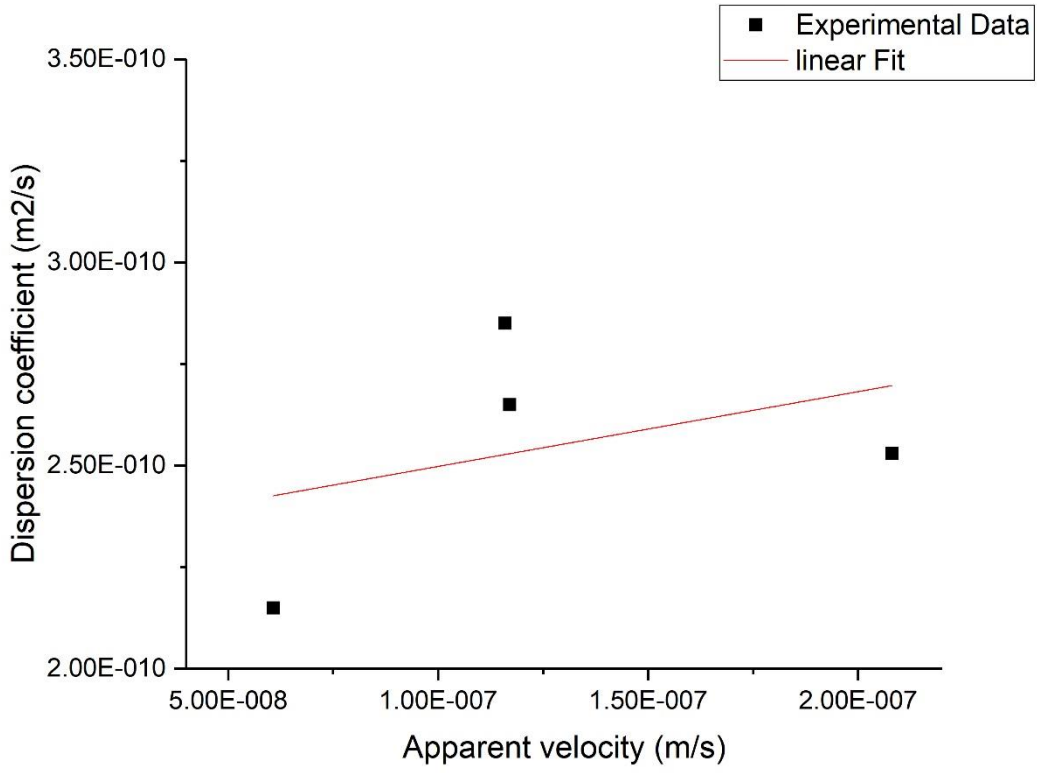

Figure 7-5: Determination of apparent diffusion coefficient of selenate ion in

bentonite with existence of silicic acid by linear regression.

From the intercept on y-axis, the apparent diffusion coefficient of selenate ion in bentonite with existence of silicic acid was derived to be 2.31×10^{-10} m^2/s.

Method 2: Nernst–Einstein relation

According to Eq. 5.15,

$$D_m^a = \mu^a \cdot \frac{kT}{Ze} = (\mu_{em}^a \pm \mu_{om}^a) \cdot \frac{kT}{Ze} = (\mu_{em}^a \pm \frac{\mu_{om}}{R \cdot \tau^2}) \cdot \frac{kT}{Ze} \quad \text{(Eq. 7.3)}$$

As for selenate ions as anodic species,

$$D_m^a = (\mu_{em}^a - \frac{\mu_{om}}{R \cdot \tau^2}) \cdot \frac{kT}{Ze} \quad \text{(Eq. 7.4)}$$

The term μ_{em}^a in the equation can be obtained from the slope of apparent convective velocity V_{app} plotting against electric field exerted E according to Eq. 5.3: $V_{em} = \mu_{em} \cdot E$.

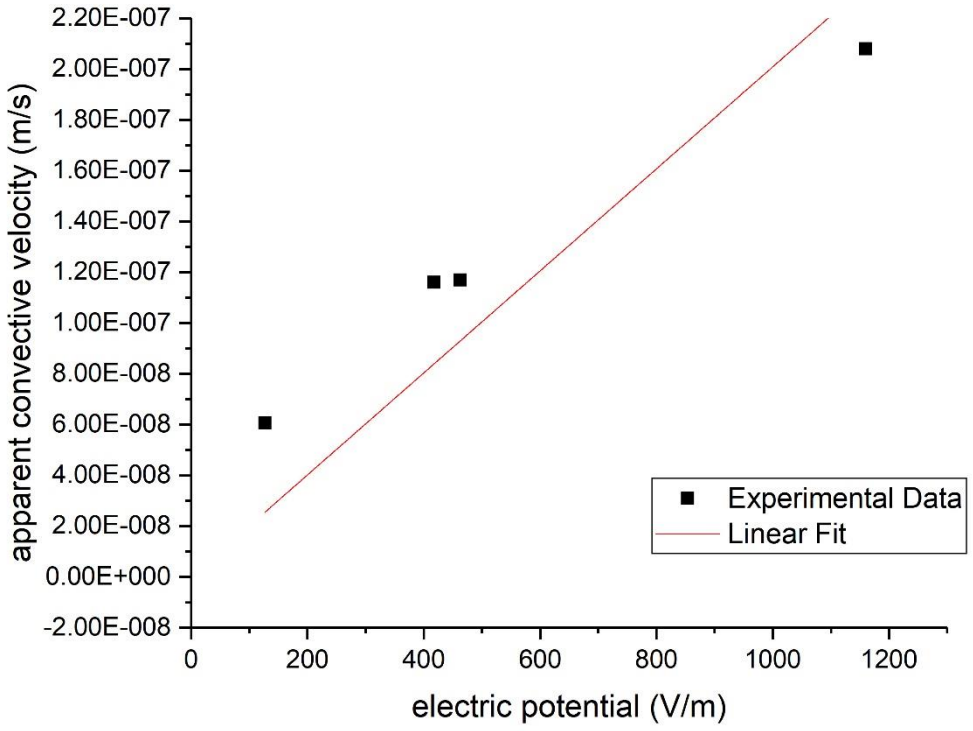

Figure 7-6: Determination of electromigration mobility of selenate ion in bentonite with existence of silicic acid by linear regression.

From linear regression, the μ_{em}^{a} was determined to be 2.01×10^{-10} $m^2/(V\cdot s)$. Then by Eq. 7.4, the apparent diffusion coefficient of selenate in bentonite can be calculated, as long as the term $\mu_{om}/(R\cdot\tau^2)$ is characterized. Such measurement can be done in electromigration experiments with HTO in bentonite at different electric fields [61]. When the apparent electroosmotic mobility is determined, a comparison of apparent diffusion coefficients obtained by hydrodynamic dispersion relation and Nernst–Einstein relation can be made.

According to the work by Hu et al. [76] and Hiemstra et al. [77], silicate ion had a high affinity to metal oxides and tend to form inner-sphere surface complexes through a mechanism of ligand exchange with surface groups. As for selenate ion, however, it was reported by researchers including Wu et al. [52] and Zhang et al. [54] that weak outer-sphere surface complexes through electrostatic attraction on surface of metal oxides. From investigations of competitive adsorption [53], they showed that anions that form inner-sphere complexes usually prevent outer-sphere complexes from forming. Hence, from theoretical aspect, existence of silicate ion is supposed to inhibit the adsorption of selenate ion on surface of metal oxides and thus facilitate the migration of selenate ion within interlayer, interparticle and interaggregate space. This prediction was hence verified by the results of experiments.

Silicic acid with a concentration of 1 mM was reported to have a pH value of approximately 6.40. Hence, existence of silicic acid not only affects sorption process of selenate ions on clay surface, but also slight modification of pH level in clay samples is anticipated. To examine such modification on pH level, measurements were conducted on clay samples saturated with 15 mM $NaHCO_3$ solution and samples saturated with a mixture of 15 mM $NaHCO_3$ and 1 mM H_4SiO_4.

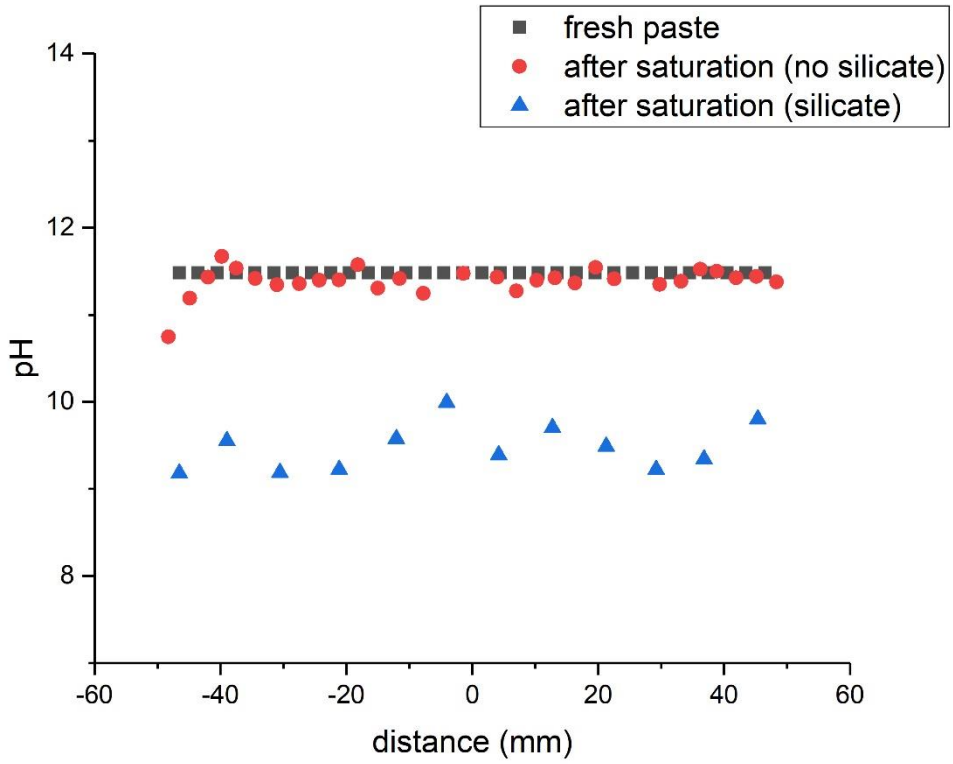

Figure 7-7: pH level of internal solution in bentonite before and after saturation.

From the results of pH measurements, it can thus be concluded that, pH level of internal solution in fresh paste of bentonite was approximately 11.5; after saturation process with 15 mM $NaHCO_3$ solution, no significant modification of pH level was observed; and after saturation process with a mixed solution with 15 mM $NaHCO_3$ and 1 mM H_4SiO_4, acidification of internal solution was observed and the modification had a scale of two pH levels.

7.1.2 Electromigration experiments conducted on Boom Clay

In the electromigration experiments conducted on Boom Clay, the inherent diffusion coefficient of selenate ion (SeO_4^{2-}) in Boom Clay was investigated.

A series of experiments were conducted, in which the current exerted during electromigration and the duration were the variables. The currents exerted were in a range of 0 to 40 mA and the duration in a range of 6 to 48 hours. The parameters adopted were designed based on a balance between maximizing varying ranges to obtain sufficient and reliable results and keeping parameters within safe limits.

For each electromigration experiment, a distribution profile was drawn with the concentrations of selenate tracer ion (SeO_4^{2-}) at different depths of clay core. The peak

location of the profile and the peak width were respectively determined by the corresponding apparent convection velocity and the dispersion coefficient. The distribution profiles of selenium concentration in Boom Clay after electromigration are displayed in Figure 7-8. A general rule can be observed from the profiles, that current applied and duration of time together decided the location of peak and longer time led to larger dispersion.

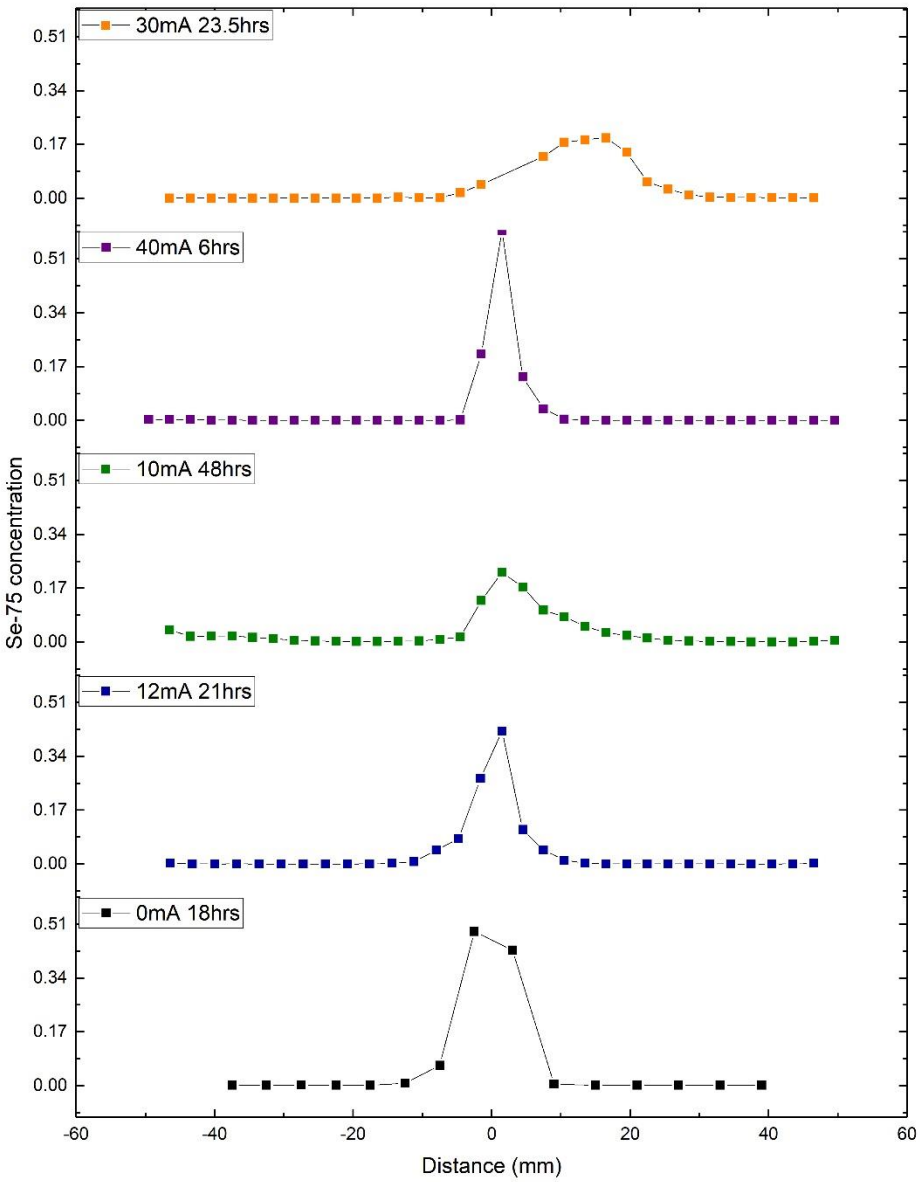

Figure 7-8: The distribution profiles of selenium concentration in Boom Clay after electromigration.

Method 1: hydrodynamic dispersion relation

By function fitting of the distribution profile with Eq. 5.9, apparent convection velocity and dispersion coefficient were calculated. The calculated apparent convection velocities and dispersion coefficients from the results of electromigration with Boom Clay are summarized in the Table 7-5 below.

Table 7-5: Apparent convection velocities and dispersion coefficients calculated from the results of electromigration with Boom Clay.

Apparent velocity m/s	**Dispersion coefficient m^2/s**	**Current mA**	**Electric field V/m**	**Duration hrs**
-7.72E-10	9.20E-11	0	-4.67	18
7.94E-09	5.30E-11	12	10.13	21
2.00E-08	9.90E-11	10	46.67	48
5.88E-08	8.80E-11	40	356.00	6
1.55E-07	2.82E-10	30	388.00	23.5

With such series of apparent velocities and dispersion coefficients, the apparent diffusion coefficient of selenate ion can then be obtained through linear regression according to Eq. 5.10.

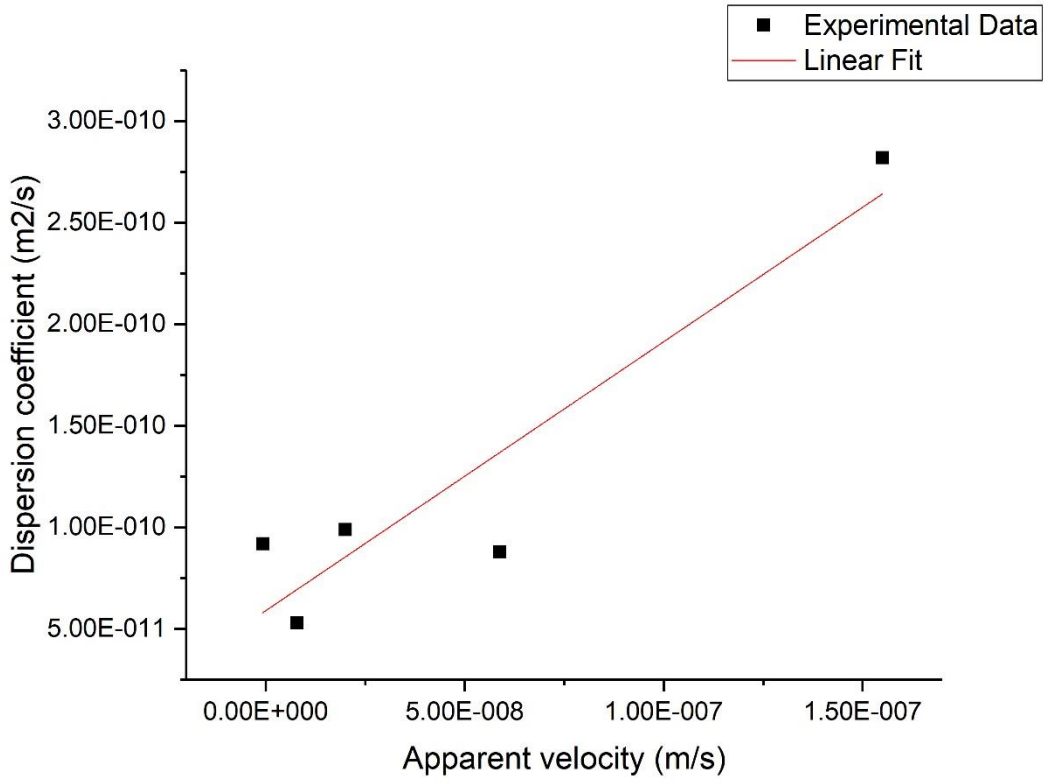

Figure 7-9: Determination of apparent diffusion coefficient of selenate ion in Boom Clay by linear regression.

From the intercept on y-axis, the apparent diffusion coefficient of selenate ion in Boom Clay was derived to be 5.90×10^{-11} m^2/s.

Method 2: Nernst–Einstein relation

According to Eq. 5.15,

$$D_m^a = \mu^a \cdot \frac{kT}{Ze} = (\mu_{em}^a \pm \mu_{om}^a) \cdot \frac{kT}{Ze} = (\mu_{em}^a \pm \frac{\mu_{om}}{R \cdot \tau^2}) \cdot \frac{kT}{Ze} \quad \text{(Eq. 7.5)}$$

As for selenate ions as anodic species,

$$D_m^a = (\mu_{em}^a - \frac{\mu_{om}}{R \cdot \tau^2}) \cdot \frac{kT}{Ze} \quad \text{(Eq. 7.6)}$$

The term $\mu_{em}{}^a$ in the equation can be obtained from the slope of apparent convective velovity V_{app} plotting against electric field exerted E according to Eq. 5.3: $V_{em} = \mu_{em} \cdot E$.

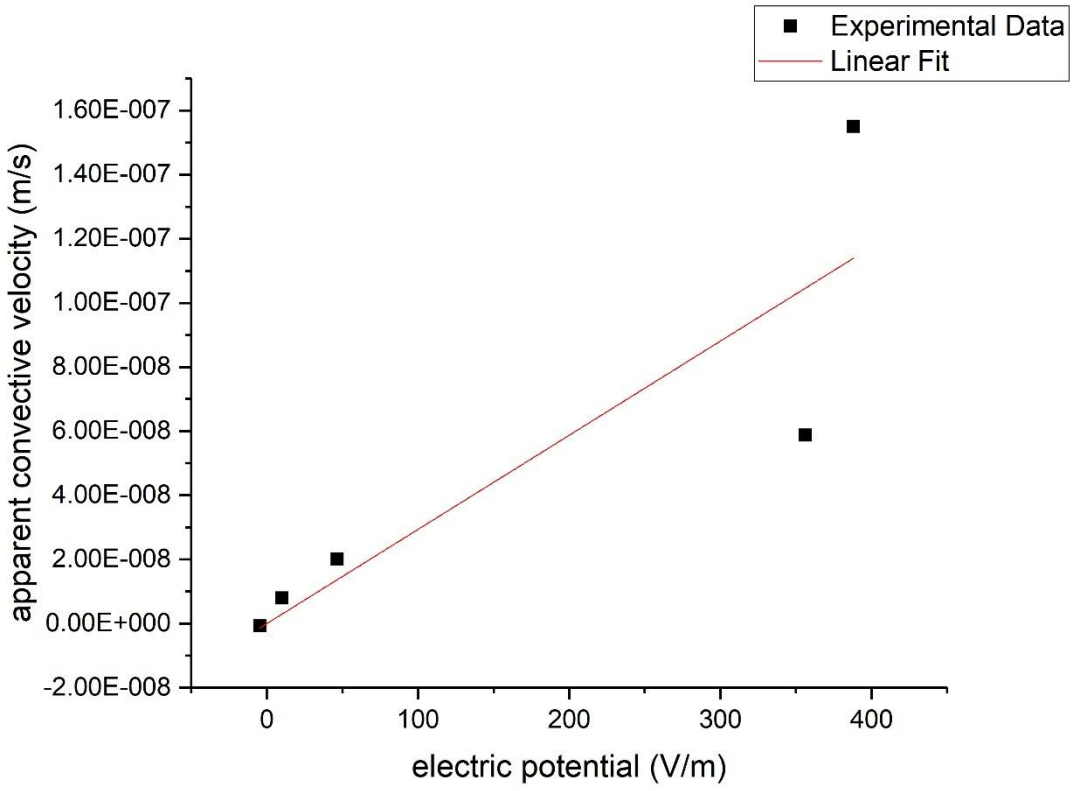

Figure 7-10: Determination of electromigration mobility of selenate ion in Boom Clay

by linear regression.

From linear regression, the μ_{em}^{a} was determined to be 2.94×10^{-10} $m^2/(V\cdot s)$. Then by Eq. 7.6, the apparent diffusion coefficient of selenate in Boom Clay can be calculated, as long as the term $\mu_{om}/(R\cdot\tau^2)$ is characterized. Such measurement can be done in electromigration experiments with HTO in Boom Clay at different electric fields [61]. When the apparent electroosmotic mobility is determined, a comparison of apparent diffusion coefficients obtained by hydrodynamic dispersion relation and Nernst–Einstein relation can be made.

Up to now, the only study that has investigated migration of selenate in argillaceous rocks is that of Beauwens et al. [63] The apparent diffusion coefficient of selenate ion in Boom Clay was determined to be 1.70×10^{-11} m^2/s from hydrodynamic dispersion relation and 6.30×10^{-11} m^2/s from Nernst-Einstein relation, for a dry density of around 1.70 g/cm^3.

The value of apparent diffusion coefficient was proven to vary with matrix differences, especially with different degree of compaction and water saturation. Such variation is hence a function of sample envolope density and can be as large as two orders of magnitude according to Ochs et al. [78, 79], Sato et al. [80] and Kim et al. [81].

The Boom Clay samples adopted in this project for electromigration has a dry density of 1.11 g/cm^3. The value of apparent diffusion coefficient was derived from hydrodynamic dispersion relation. Hence from a comparison, the results are in the same order of magnitude while some divergence is caused by difference in dry density. Consequently, a conclusion can be drawn that the results derived have a good reliability and agree with the results obtained by other researchers.

It was also reported by some researchers that migration or adsorption of sulphate ion resembled to migration or adsorption of selenate ion on metal oxide surface [57, 75]. Yet seldom investigation has been conducted on sulphate behaviour in Boom Clay as well.

7.2 Chemical characterizations

Instrumental neutron activation analysis (INAA) was conducted at Reactor Institute Delft to obtain an accurate elemental composition of pure Boom Clay. Absolute concentrations of various elements are given below:

Table 7-6: Absolute concentrations of elements measured by INNA in the Boom Clay sample.

Element	Concentration (mg/kg)	Detection limit	Element	Concentration (mg/kg)	Detection limit

		(mg/kg)			(mg/kg)
Na	5.04E+03	3.3E+00	Mg	1.35E+04	9.0E+02
Al	8.08E+04	l.0E+03	Si	3.0E+05	2.1E+05
Cl	4.06E+03	9.8E+01	K	2.73E+04	2.9E+02
Ca	6.6E+03	1.7E+03	Sc	1.64E+01	2.3E-02
Ti	5.1E+03	2.8E+02	V	1.47E+02	4.1E+00
Cr	1.22E+02	2.1E+00	Mn	1.78E+02	1.5E+00
Fe	4.95E+04	10E-01	Co	1.71E+01	4.2E-01
Ni	-	1.9E+02	Cu	-	1.7E+02
Zn	1.35E+02	1.1E+01	Ga	2.2E+01	3.4E+00
As	1.20E+01	5.3E-01	Se	-	2.8E+00
Br	2.27E+01	4.3E-01	Rb	1.39E+02	1.1E+01
Sr	-	1.2E+02	Zr	2.7E+02	1.1E+02
Mo	-	3.5E+01	Ru	-	1.9E+00
Pd	-	6.1E+01	Ag	-	8.6E+00
Cd	-	9.9E+00	In	-	1.3E-01
Sn	-	7.7E+01	Sb	-	2.4E+00
I	8E+00	6.1E+00	Cs	5.04E+01	4.2E-01
Ba	3.2E+02	7.9E+01	La	3.75E+01	1.1E-01
Ce	8.4E+01	9.3E-01	Nd	3.0E+01	3.7E+00
Sm	6.25E+00	1.1E-01	Eu	1.27E+00	5.2E-02
Tb	7.7E-01	1.6E-01	Dy	4.5E+00	7.5E-01
Ho	-	5.0E+00	Yb	2.74E+00	2.0E-01
Lu	3.8E-01	4.0E-02	Hf	5.7E+00	2.3E-01
Ta	1.15E+00	1.9E-01	W	2.3E+00	6.3E-01
Re	-	1.4E-01	Pt	-	8.6E+00
Au	-	5.9E-02	Th	2.94E+01	1.9E-01
U	2.7E+00	7.5E-01			

Hence, the main constituent elements are (in percentage):

Table 7-7: Main elements composing the Boom Clay sample.

Si	Al	Fe	K	Mg	Ca	Ti	Na
60.73	16.36	10.02	5.53	2.73	1.34	1.03	1.02
Cl	Ba	Zr	Mn	V	Rb	Zn	Cr
0.82	0.06	0.05	0.04	0.03	0.03	0.03	0.02

The results are matching the results obtained from semi-quantitative analysis of XRF (Table 6-2). In future experiments, the same characterization would be as well conducted on Boom Clay samples that undergo concrete/clay interactions. Comparisons with this original composition would be made to investigate the depletion or enrichment phenomena at concrete/clay interactions, of which the existence was

reported by various researchers [82, 83].

7.3 Pore structure characterizations

Mercury intrusion porosimetry (MIP) test was conducted with a cubic Boom Clay sample obtained from the inner part of clay core with a mass of 1.80 g. With intrusion and extrusion of mercury in the clay sample, various important parameters were obtained.

Table 7-8: Summary of parameters measured by MIP test.

Total intrusion volume	0.1424	mL/g
Total pore area	9.179	m^2/g
Median pore diameter (volume)	0.2242	µm
Median pore diameter (area)	0.0198	µm
Average pore diameter	0.0621	µm
Bulk density at 0.0037 MPa	1.9326	g/mL
Apparent (skeletal) density	2.6666	g/mL
Porosity	27.5235	%
Permeability constant	0.00442	
Permeability	111.1098	mdarcy
BET surface area	230.0000	m^2/g
Pore shape exponent	1.00	
Tortuosity factor	2.125	
Tortuosity	10.6931	
Percolation fractal dimension	2.790	
Backbone fractal dimension	2.560	

It is worth mentioning that the parameters obtained for Boom Clay pore structure are restricted by the detection limit of MIP technique which is approximately 7 nm. According to research by Kuila et al. [84], size of pores in most clays and shales lie in a range of 1-300 nm.

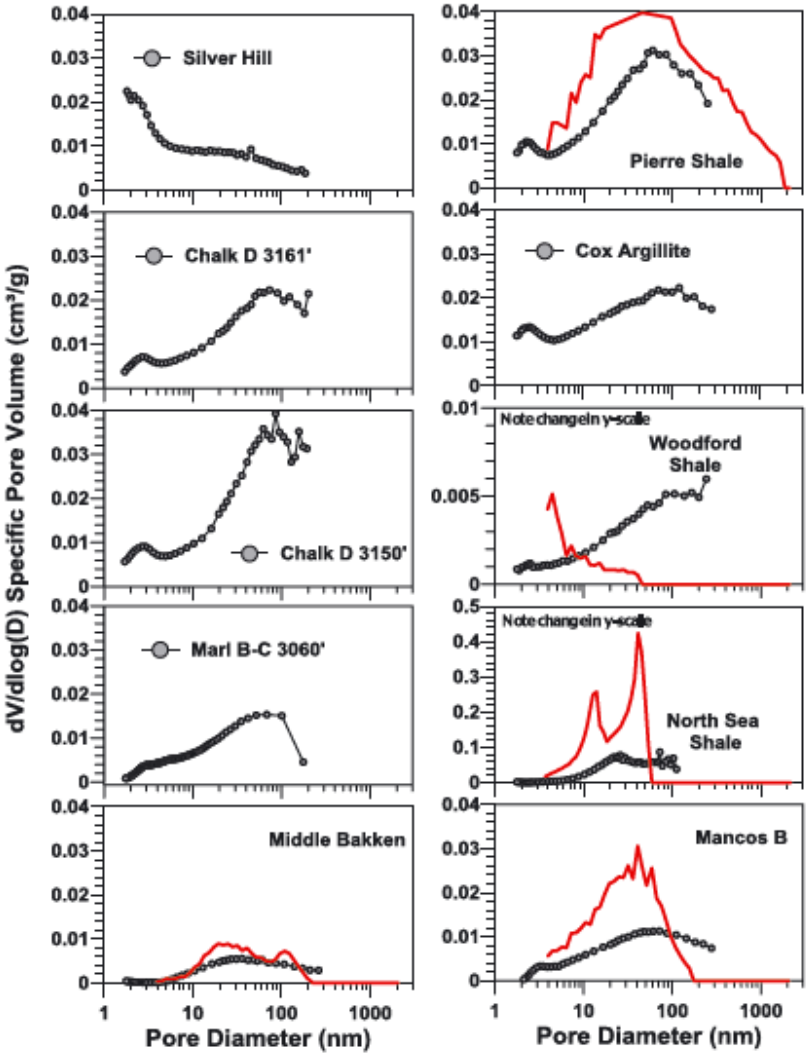

Figure 7-11: Pore size distribution of the clay and shale samples obtained by nitrogen adsorption isotherm (black) and MIP (red) [84].

Compared to the results obtained by researchers from SCK·CEN, density parameters are matching well while mercury intrusion porosity data is not available for comparison [36].

Table 7-9: Comparison of results from this project and from SCK·CEN.

Parameter	This project	SCK·CEN	Unit
Bulk density	1.9326	1.9-2.1	g/mL
Apparent density	2.6666	2.65	g/mL
MIP porosity	27.5235	-	%
Porosity from migration experiments	-	36-40	%

A diagram of specific pore volume dv/dlog(D) was plotted to evaluate pore size

distribution of the Boom Clay sample.

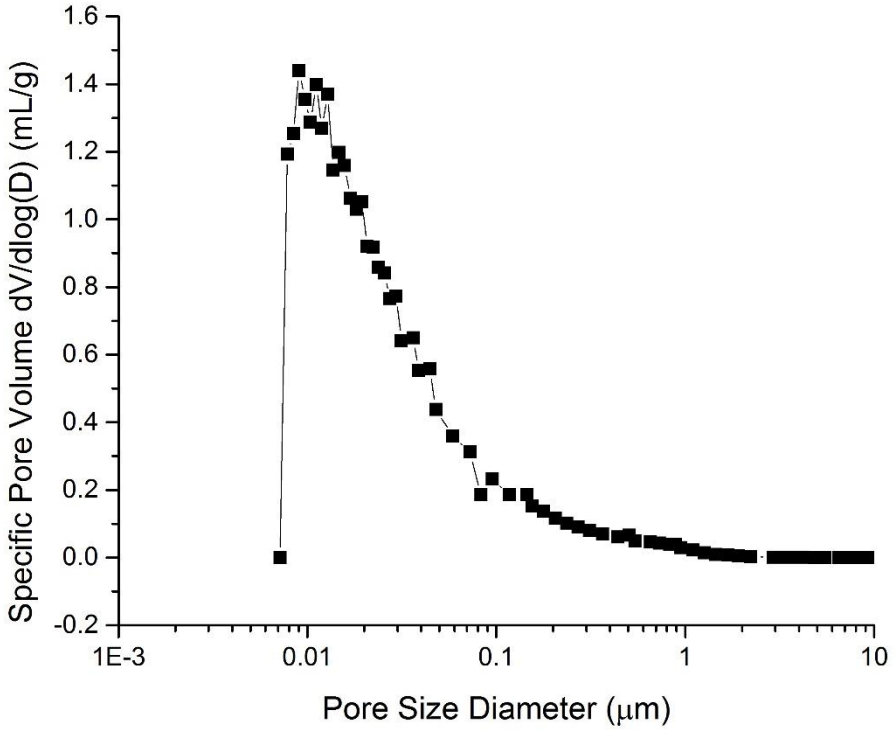

Figure 7-12: Pore size distribution of Boom Clay sample characterized by MIP technique.

From this diagram, we can see the dominant pore size is located at 10 nm and most of the pores lie in the range of 10-1000 nm. However, a steep drop of the curve at pore size of 7 nm is observed and it is believed to be the detection limit of MIP technique.

To obtained a complete idea of Boom Clay pore structure, further characterization for pores smaller than 10 nm is necessary.

In future experiments, the same characterization would be as well conducted on Boom Clay samples that undergo concrete/clay interactions. Comparisons with this original pore structure would be made to investigate the clogging phenomenon, of which the existence was reported by various researchers [82, 83, 85-87].

8 Conclusions and outlook

8.1 Conclusions

By various experiments conducted in this project, following conclusions were drawn:

(1) Apparent diffusion coefficient of selenate ion in bentonite was calculated by experimental data obtained from electromigration experiments in this project and by work of the predecessor based on hydrodynamic dispersion relation. The calculated value of apparent diffusion coefficient is 5.71×10^{-11} m^2/s.

(2) Apparent diffusion coefficient of selenate ion in bentonite with existence of silicate was calculated by experimental data obtained from electromigration experiments in this project and by work of the predecessor based on hydrodynamic dispersion relation. The calculated value of apparent diffusion coefficient is 2.31×10^{-10} m^2/s.

(3) According to apparent diffusion coefficients obtained from experiments in bentonite with and without existence of silicate, function of silicate ion facilitating migration of selenate ion in bentonite was verified.

(4) Apparent diffusion coefficient of selenate ion in Boom Clay samples with an average dry density of 1.11 g/cm^3 was calculated by experimental data obtained from electromigration experiments based on hydrodynamic dispersion relation. The calculated value of apparent diffusion coefficient is 5.90×10^{-11} m^2/s.

(5) In electromigration experiments conducted either in bentonite or in Boom Clay, a direct linear relation of electric fields exerted during electromigration and resulting apparent diffusion coefficients was observed. The values of electromigration mobility of selenate ion in bentonite, in bentonite with existence of silicate and in Boom Clay were obtained by the slopes of D^a-E curves. They are respectively 4.04×10^{-10} $m^2/(V\cdot s)$ in bentonite, 2.01×10^{-10} $m^2/(V\cdot s)$ in bentonite with existence of silicate, and 2.94×10^{-10} $m^2/(V\cdot s)$ in Boom Clay.

(6) An accurate elemental composition of pure Boom Clay was characterised by instrumental neutron activation analysis (INAA). Main elements composing Boom Clay are Si, Al, Fe, K, Mg, Ca, Ti, Na, etc.

(7) A measurement of pore structure in original Boom Clay core was conducted by technique of mercury intrusion porosimetry (MIP). Within the range of detection limits, sizes of pores mostly lie in a range of 10-1000 nm and peak at 10 nm. Other important parameters including total porosity, bulk density, apparent density, permeability and tortuosity were measured by MIP simultaneously.

8.2 Outlook

(1) As reported by previous researches, apparent diffusion coefficient in electromigration experiments can as well be calculated based on Nernst–Einstein relation apart from hydrodynamic dispersion relation. With data of electromigration mobility of selenate ion obtained from this project, data of corresponding electroosmosis mobility is not yet available. Hence, in future research, additional electromigration experiments with HTO in bentonite and Boom Clay can be conducted to make calculations based on Nernst–Einstein relation possible. At that time, a comparison between values of apparent diffusion coefficients obtained from hydrodynamic dispersion relation and Nernst–Einstein relation can be made.

(2) Due to difficulties in sampling of original Boom Clay samples led by existence of large number of voids and crevices, Boom Clay samples adopted in electromigration experiments were prepared from grinded Boom Clay powder. A difference between Boom Clay samples prepared and original Boom Clay samples in density and pore structure is resulted. To give more reliable suggestions on Dutch geological repository in the future, experiments shall be conducted with original Boom Clay samples or accurate correction shall be made on the differences.

(3) To investigate possible alternations that alkaline concrete pore water can bring to the microstructure and elemental distribution in Boom Clay, chemical characterizations (INAA) and structural characterizations (MIP) can be conducted on Boom Clay samples that are subjected to contact with an alkaline solution. By comparing with original elemental composition and original pore structure obtained in this project, type and extent of alternations are then able to obtain.

(4) To better understand complicated migration processes of selenium, which has various redox states under different conditions, in bentonite and Boom Clay, simulation work can also be conducted based on transport models and/or chemical models. Comparisons between experimental data and simulation results can be made.

Appendix A. Synthetic Boom Clay pore water

A.1. Synthetic Boom Clay pore water (SCK·CEN)

Table A-1: Composition of synthetic Boom Clay pore water (SCK·CEN)

Species	**Mean concentration (ppm)**
F^-	3.6
Cl^-	27
SO_4^{2-}	0.2
Br^-	0.49
HPO_4^{2-}	3.8
HCO_3^-	828
B	7.5
Na^+	408
Mg^{2+}	2.9
Al^{3+}	0.08
Si	5
K^+	11
Ca^{2+}	4.0
Fe^{2+}	0.9

A.2. Synthetic Boom Clay pore water (COVRA)

For the reason that the Netherlands has not yet decided on the location of repository site, no data of in situ composition of Boom Clay pore water is available. A rough composition of boom clay pore water, calculated based on a series of assumptions, was provided by the company COVRA and adopted in this project.

Table A-2: Composition of synthetic Boom Clay pore water COVRA)

Salt	**g /kg water**	**Composition of a synthetic Dutch Boom Clay pore water**	
		Anions	**mol / kg water**
NaCl	24.476	F^-	9.16E-05
$MgCl_2$	5.137	Cl^-	5.57E-01
Na_2SO_4	4.107	Br^-	8.58E-04
$CaCl_2$	1.177	SO_4^{2-}	2.89E-02
KCl	0.712	HCO_3^-	9.10E-03
$NaHCO_3$	0.656	I^-	5.91E-06
KBr	0.102	**Cations**	**mol / kg water**

H_3BO_3	0.043	Na^+	4.85E-01
NaF	0.0038	K^+	1.13E-02
$FeCl_3$	0.011	Ca^{2+}	1.06E-02
		Mg^{2+}	5.39E-02
		Fe^{3+}	6.86E-05
		Al^{3+}	2.59E-06
KI	0.010		
$AlCl_3$	0.0003	**Neutral species**	**mol / kg water**
Silicafume (amorphous silica) EMSAC 500 S	saturated	H_2SiO_3	6.96E-04
		$B(OH)_3$	1.95E-03

To work with oxidation sensitive Boom Clay, the synthetic Boom Clay pore water was as well prepare in an anaerobic environment and the deionized water used was degassed by bubbling argon overnight before use.

Appendix B. Matlab calculation script

```
ActivityData=xlsread('EXP');
xData=ActivityData(1:30,1);
cData=ActivityData(1:30,2);
cTot=sum(cData);
cNorm=cData/cTot;
//Read data from excel document and normalize.

diameter=0.03;
x=xData.*0.001;
s=(diameter.^2).*0.25.*pi;
t=7.*3600;
//Calculate time in seconds, distance in meters and cross section area of sample.

xmax=find(cData==max(cData));
Vapp=(xData(xmax).*0.001)./t;
//Search for at which location tracer has the highest concentration after electromigration and calculate the apparent velocity whereby.

DmStep=1e-12;
[Dm]=1e-11;
[E]=100;
//Set step size of calculation.

for i=(2:1e5);
Dm(i)=Dm(i-1)+DmStep;
end

for i=(1:1e5);
c_calc1=(cTot./(2.*s.*sqrt(pi.*Dm(i).*t))).*exp(-((x-Vapp.*t).^2)./(4.*Dm(i).*t));
c_calcTot1=sum(c_calc1);
c_calcNorm1=c_calc1/c_calcTot1;
E(i)=sum((c_calcNorm1-cNorm).^2);
end
//Calculate curves of concentration distribution at each step. Calculate variance with the measured curve at each step.

I=find(E==min(E));
Di=Dm(I);
//Find the curve with smallest variance value and the Dm at that step is the dispersion coefficient.

c_calc2=(cTot./(2.*s.*sqrt(pi.*Di.*t))).*exp(-((x-Vapp.*t).^2)./(4.*Di.*t));
```

```
c_calcTot2=sum(c_calc2);
c_calcNorm2=c_calc2/c_calcTot2;

figure;
plot(x,cNorm,'-*',x,c_calcNorm2,'-o');
legend('measured','calculated');
ylabel('c/c_0');
xlabel('x [m]');
//Calculate and plot the calculated curve along with the measured one.
```

Appendix C. Labview script

<VI syntaxVersion=11 LVversion=12008004 revision=35 name="ReadVoltage.vi">
<TITLE><NO_TITLE name="ReadVoltage.vi"></TITLE>
<HELP_PATH></HELP_PATH>
<HELP_TAG></HELP_TAG>
<RTM_PATH type="default"></RTM_PATH>
<DESC></DESC>
<CONTENT>
<GROUPER>
<PARTS>
</PARTS></GROUPER>
<CONTROL ID=83 type="Cluster" name="error out">
<DESC><<B>>error in<</B>> can accept error information wired from VIs previously
called. Use this information to decide if any functionality should be bypassed in the event of
errors from other VIs.<LF>
<LF> RightZclick the <<B>>error in<</B>> control on the front panel and select
<<B>>Explain Error<</B>> or <<B>>Explain Warning<</B>> from the shortcut menu for
more information about the error.</DESC>
<TIP></TIP>
<PARTS>
<PART ID=82 order=0 type="Caption"><LABEL><STEXT>error
out</STEXT></LABEL></PART>
</PARTS>
<CONTENT>
(checkmark) to indicate a warning or that no error occurred.<LF>
<LF> RightZclick the <<B>>error in<</B>> control on the front panel and select
<<B>>Explain Error<</B>> or <<B>>Explain Warning<</B>> from the shortcut menu for
more information about the error.</DESC>
<TIP></TIP>
<PARTS>
<PART ID=22 order=0 type="Boolean
<GROUPER>
<PARTS>
</PARTS></GROUPER> <CONTROL ID=79 type="Boolean" name="status">
<DESC><<B>>status<</B>> is TRUE (X) if an error occurred or FALSE
Text"><MLABEL><STRINGS><STRING></STRING><STRING></STRING><ST
RING
></STRING><STRING></STRING></S TRINGS></MLABEL></PART>
<PART ID=82 order=0

type="Caption"><LABEL><STEXT>status</STEXT></LABEL></PART>
<LF> RightZclick the <<B>>error in<</B>> control on the front panel and select <<B>>Explain Error<</B>> or <<B>>Explain Warning<</B>> from the shortcut menu for
more information about the error.</DESC>
</PARTS>
</CONTROL>
<CONTROL ID=80 type="Numeric" name="code">
<DESC><<B>>code<</B>> is the error or warning code.<LF>
type="Caption"><LABEL><STEXT>code</STEXT></LABEL></PART>
33
<TIP></TIP>
<PARTS>
<PART ID=82 order=0
<LF> RightZclick the <<B>>error in<</B>> control on the front panel and select <<B>>Explain Error<</B>> or <<B>>Explain Warning<</B>> from the shortcut menu for
more information about the error.</DESC>
</PARTS>
</CONTROL>
<CONTROL ID=81 type="String" name="source">
<DESC><<B>>source<</B>> describes the origin of the error or warning.<LF>
type="Text"><LABEL><STEXT></STEXT></LABEL></PART>
<PART ID=82 order=0
type="Caption"><LABEL><STEXT>source</STEXT></LABEL></PART>
<TIP></TIP>
<PARTS>
<PART ID=11 order=0
</CONTENT> </CONTROL>
</PARTS>
<DEFAULT><SAME_AS_LABEL></DEFAULT> </CONTROL>
<CONTROL ID=94 type="Waveform Chart" name="Waveform Chart">
<DESC></DESC>
<TIP></TIP>
<PARTS>
color=000000>
Chart</STEXT></LABEL></PART>
<PART ID=8022 order=0 type="">
<CONTROL ID=231 type="Tree" >
<DESC></DESC>
<TIP></TIP>
<PARTS>
<GROUPER>
<PARTS>

</PARTS></GROUPER> </PARTS>
</CONTROL> </PART>
</CELL_FONTS> <ROW_HEADER> </ROW_HEADER> <COL_HEADER>
<STRING>Cursors:</STRING> <STRING>X</STRING> <STRING>Y</STRING>
</COL_HEADER> <STRINGS> </STRINGS>
<PRIV>
<CELL_FONTS>
[Z2 Z2]<FONT predef=APPFONT color=000000> [Z1 Z2]<FONT predef=APPFONT
style='B'
34
</PRIV>
<PART ID=82 order=0 type="Caption"><LABEL><STEXT>Waveform
<SCALE_NAMES><STRING>Time</STRING><STRING>Amplitude</STRING>
</SCA
LE_NAMES>
</PRIV>
</PARTS>
<PRIV>
<PLOTS><STRING>Plot 0</STRING></PLOTS>
</CONTROL>
<CONTROL ID=79 type="Boolean" name="stop">
color=FF0000><STRINGS><STRING>STOP</STRING><STRING>STOP</STRI
NG><S
TRING>STOP</STRING><STRING>S
TOP</STRING></STRINGS></MLABEL></PART>
</PRIV>
<DESC></DESC>
<TIP></TIP>
<PARTS>
<PART ID=22 order=0 type="Boolean Text"><MLABEL><FONT predef=SYSFONT
<PART ID=82 order=0 type="Caption"><LABEL><STEXT><FONT
predef=DLGFONT color=100000C>stop</STEXT></LABEL></PART>
</PARTS>
</CONTROL>
<CONTROL ID=91 type="Path" name="data file:">
<DESC></DESC>
<TIP></TIP>
<PARTS>
type="Text"><LABEL><STEXT>c:\users\data\test.bin</STEXT></LABEL></PART>
<PART ID=82 order=0 type="Caption"><LABEL><STEXT>data
file:</STEXT></LABEL></PART>
</PARTS>
<PRIV>
<PART ID=8019 order=0 type="Browse Button"> <CONTROL ID=79

type="Boolean"
>
</CONTROL> </PART>
<PART ID=11 order=0
<DESC></DESC> <TIP></TIP> <PARTS> </PARTS>
<PROMPT></PROMPT>
<MTCH_PTN></MTCH_PTN>
<PTN_LBEL></PTN_LBEL>
<STRT_PTH><PATH type="absolute"></PATH></STRT_PTH>
<PTH_BTN_LBL></PTH_BTN_LBL>
</CONTROL>
<CONTROL ID=80 type="Numeric" name="output 1">
1</STEXT></LABEL></PART>
35
</PARTS>
</CONTROL> </CONTENT>
<BDCONTENT>
<CONTROL ID=81 type="String Constant" name="format (%.3f)"> <DESC></DESC>
<TIP></TIP>
<PARTS>
<PART ID=11 order=0
type="Text"><LABEL><STEXT>%.5f</STEXT></LABEL></PART> </PARTS>
<DEFAULT><SAME_AS_LABEL></DEFAULT>
</CONTROL>
<CONTROL ID=81 type="String Constant" name="delimiter (\t)"> <DESC></DESC>
<TIP></TIP>
<PARTS>
<PART ID=11 order=0
type="Text"><LABEL><STEXT>,</STEXT></LABEL></PART> </PARTS>
<DEFAULT><SAME_AS_LABEL></DEFAULT>
</CONTROL>
<CONTROL ID=79 type="False Constant" name="append to file? (new file:F)">
<DESC></DESC>
<TIP></TIP>
<PARTS>
</PARTS>
</CONTROL>
<NODE ID=197 type="PolyVI" subVIName="Write To Spreadsheet File.vi">
<DESC></DESC>
</NODE>
<NODE ID=47 type="Function" primID=53544446 primName="Format Date/Time String">
<DESC></DESC>
</NODE>

<NODE ID=47 type="Function" primID=20503253 primName="String To Path">
<DESC></DESC>
</NODE>
<NODE ID=62 type="Concatenate Strings">
<DESC></DESC>
</NODE>
<CONTROL ID=81 type="String Constant" >
<DESC></DESC>
<TIP></TIP>
<PARTS>
<PART ID=11 order=0
type="Text"><LABEL><STEXT></STEXT></LABEL></PART>
</PARTS>
<DEFAULT><STRING>d:\</STRING></DEFAULT>
</CONTROL>
<CONTROL ID=81 type="String Constant" >
<DESC></DESC>
<TIP></TIP>
<PARTS>
36
<PART ID=11 order=0
type="Text"><LABEL><STEXT>.csv</STEXT></LABEL></PART> </PARTS>
<DEFAULT><SAME_AS_LABEL></DEFAULT>
</CONTROL>
<NODE ID=62 type="Concatenate Strings">
<DESC></DESC>
</NODE>
<CONTROL ID=81 type="String Constant" name="time format string (%c)">
<DESC></DESC>
<TIP></TIP>
<PARTS>
<PART ID=11 order=0
type="Text"><LABEL><STEXT></STEXT></LABEL></PART>
</PARTS>
<DEFAULT><STRING>%y%m%d%H%M</STRING></DEFAULT>
<DEFAULT>
<PATH type="absolute">c<SEP>users<SEP>data<SEP>test.bin</PATH>
</DEFAULT>
<DESC></DESC>
<TIP></TIP>
<PARTS>
<PART ID=82 order=0 type="Caption"><LABEL><STEXT>output
</CONTROL>
<CONTROL ID=85 type="VISA resource name" name="VISA resource name">

<DESC></DESC>
<TIP></TIP>
<PARTS>
</PARTS>
</CONTROL>
<PART ID=8017 order=0 type="I/O Name Display">
<CONTROL ID=148 type="VISA USB Control Out" >
</CONTROL> </PART>
<NODE ID=33 type="While Loop">
<DESC></DESC>
<BDCONTENT>
type="Text"><LABEL><STEXT>%f</STEXT></LABEL></PART>
primName="Equal?">
Read STB">
FETCH?</STEXT></LABEL></PART>
<DESC></DESC> <TIP></TIP> <PARTS> </PARTS>
<CONTROL ID=80 type="Numeric Constant" name="milliseconds to wait">
<DESC></DESC>
<TIP></TIP>
<PARTS>
</PARTS>
</CONTROL> <NODE ID=47 type="Function" primID=54494157 primName="Wait (ms)"> <DESC></DESC>
</NODE> <CONTROL ID=81 type="String Constant" name="format string">
<DESC></DESC>
<TIP></TIP>
37
<PARTS>
<PART ID=11 order=0
</PARTS>
<DEFAULT><SAME_AS_LABEL></DEFAULT> </CONTROL> <NODE ID=146 type="Scan From String">
<DESC></DESC>
</NODE>
<NODE ID=33 type="While Loop">
<DESC></DESC>
<BDCONTENT>
<CONTROL ID=80 type="Numeric Constant" name="y"> <DESC></DESC>
<TIP></TIP>
<PARTS>
</PARTS>
</CONTROL> <NODE ID=47 type="Function" primID=20205145
<DESC></DESC>
</NODE> <NODE ID=47 type="Function" primID=42545356 primName="VISA

</BDCONTENT>
</NODE> <CONTROL ID=81 type="String Constant" name="write buffer">
<DESC></DESC> </NODE>
<DESC></DESC>
<TIP></TIP>
<PARTS>
<PART ID=11 order=0 type="Text"><LABEL><STEXT>INIT<LF>
</PARTS>
<DEFAULT><SAME_AS_LABEL></DEFAULT>
</CONTROL> <NODE ID=47 type="Function" primID=54525756 primName="VISA
Write"> <DESC></DESC>
</NODE>
<CONTROL ID=80 type="Numeric Constant" name="byte count">
<DESC></DESC> <TIP></TIP> <PARTS>
</BDCONTENT>
</NODE>
<NODE ID=33 type="While Loop">
<DESC></DESC>
<BDCONTENT>
</BDCONTENT>
</NODE>
</PARTS>
</CONTROL> <NODE ID=47 type="Function" primID=20445256 primName="VISA
Read"> <DESC></DESC>
</NODE>
<CONTROL ID=80 type="Numeric Constant" name="y"> <DESC></DESC>
<TIP></TIP>
<PARTS>
</PARTS>
38
</CONTROL> <NODE ID=47 type="Function" primID=20205145 primName="Equal?">
<DESC></DESC>
</NODE> <NODE ID=47 type="Function" primID=42545356 primName="VISA Read
STB"> <DESC></DESC>
</NODE>
<CONTROL ID=81 type="String Constant" name="write buffer">
CONF:VOLT:DC<LF> TRIG:SOUR IMM<LF> *OPC</STRING></DEFAULT>
</CONTROL>
<DESC></DESC>
<TIP></TIP>

<PARTS>
<PART ID=11 order=0 type="Text"><LABEL><STEXT></STEXT></LABEL></PART>
</PARTS>
<DEFAULT><STRING>*ESE 1<LF>
<NODE ID=47 type="Function" primID=54525756 primName="VISA Write">
<DESC></DESC>
</NODE>
<CONTROL ID=81 type="String Constant" name="write buffer">
</CONTROL>
<NODE ID=47 type="Function" primID=534C4356 primName="VISA Close">
<DESC></DESC>
<DESC></DESC>
<TIP></TIP>
<PARTS>
<PART ID=11 order=0 type="Text"><LABEL><STEXT></STEXT></LABEL></PART>
</PARTS>
<DEFAULT><STRING>*CLS</STRING></DEFAULT>
</NODE>
<NODE ID=47 type="Function" primID=54525756 primName="VISA Write">
<DESC></DESC>
</NODE>
<NODE ID=47 type="Function" primID=524C4356 primName="VISA Clear">
<DESC></DESC>
</NODE>
</BDCONTENT>
</VI>

Appendix D. Calculation of clay dry density

Dry density of clay, which is a reflect of clay porosity or degree of compaction, is reported to has a direct effect on apparent diffusion coefficient of clay [78-81]. To better make comparisons with other researches, the dry density of clay used in this project is determined.

In the test, the dry density cannot be determined directly. To determine the dry density, the grain density of clay in needed to be determined first.

Traditionally, grain density is determined in pycnometers, but for swelling clays this is problematic. Grain density of clay is determined with the guidance of a technical report by Karnland et al. [88]. Approximately 20 g of different Boom Clay samples were first dried at 105 °C in a ventilated oven for 24 hours to completely remove adsorbed water in clay samples. After drying, the samples were taken out of the oven and poured into the volumetric flasks quickly, then sealed, cooled to room temperature and weighed (m_{s+f}). Small amount of water was added to the flask to completely immerse the dried clay samples. Then flasks were sealed and shaken for one hour to facilitate eliminating air. After that, the flasks were kept still for 24 hours until shaken once again. The volumetric flasks were filled with water until full then weighed again (m_{tot}).

The grain density could then be calculated with equation:

$$\rho_g = \frac{m_s}{V_{tot} - \frac{m_{tot} - m_{s+f}}{\rho_w}} \quad \text{(Eq. D.1)}$$

where m_s is the mass of the clay sample after drying [g], V_{tot} is the total volume of the volumetric flask [cm^3], m_{tot} is the total mass of clay, water and flask [g], m_{s+f} is the mass of clay and flask [g] and ρ_w is the density of water [g/cm^3].

With grain density determined, the dry density can then be calculated:

$$\rho_d = \frac{\rho_g \cdot \rho_w}{\rho_g \cdot w + \rho_w} \quad \text{(Eq. D.2)}$$

where ρ_g is the grain density [g/cm^3], as calculated previously, ρ_w is the density of water [g/cm^3] and w is the wat er ratio [-] and is calculated by:

$$w = \frac{m_w}{m_s} \quad \text{(Eq. D.3)}$$

where m_w is the mass loss during drying [g] and m_s is the remaining mass of the clay sample [g].

Reference

1. *World Nuclear Performance Report 2017*. 2017; Available from: http://www.world-nuclear.org/our-association/publications/online-reports/world-nuclear-performance-report.aspx.
2. AGENCY, I.A.E., *Classification of Radioactive Waste*. IAEA Safety Standards Series. 2009, Vienna: INTERNATIONAL ATOMIC ENERGY AGENCY.
3. Kerrisk, J.F., *Assessment of the important radionuclides in nuclear waste*. 1985, Los Alamos National Lab., NM (United States).
4. Murray, R.L. and K.E. Holbert, *Chapter 23 - Radioactive waste disposal*, in *Nuclear Energy (Seventh Edition)*. 2015, Butterworth-Heinemann: Boston. p. 395-426.
5. Saeb, S. and S.J. Patchet, *Radioactive Waste Disposal (Geology) A2 - Meyers, Robert A*, in *Encyclopedia of Physical Science and Technology (Third Edition)*. 2003, Academic Press: New York. p. 633-641.
6. Crossland, I., *18 - Disposal of radioactive waste*, in *Nuclear Fuel Cycle Science and Engineering*. 2012, Woodhead Publishing. p. 531-557.
7. Chapman, N. and A. Hooper, *The disposal of radioactive wastes underground.* Proceedings of the Geologists' Association, 2012. **123**(1): p. 46-63.
8. Delay, J., et al., *Making of the underground scientific experimental programme at the Meuse/Haute-Marne underground research laboratory, north eastern France.* Physics and Chemistry of the Earth, Parts A/B/C, 2007. **32**(1): p. 2-18.
9. Dvořáková, M., M. Vencl, and T. Bečvaříková. *Deep geological repository for disposal of nuclear waste in the Czech Republic*. in *Energy (IYCE), 2015 5th International Youth Conference on*. 2015. IEEE.
10. Council, N.R., *The disposal of radioactive waste on land.* 1957.
11. Polvani, C., *Objectives, concepts and strategies for the management of radioactive waste arising from nuclear power programmes.* Report by a Group of Experts of the OECD Nuclear Energy Agency, OECD/NEA, Paris, 1977. **153**.
12. Svensk, K.A., *Final storage of spent nuclear fuel-KBS-3.* 1983.
13. Johnson, L., et al., *The disposal of Canada's nuclear fuel waste: the vault model for postclosure assessment*. 1994, Atomic Energy of Canada Limited.
14. Dossier, A., *Argile: Évaluation de la Faisabilité du Stockage Géologique en Formation Argileuse. Document du Synthèse*. 2005, Andra, Paris.
15. Apted, M. *Robust EBS design and source-term analysis for the partially saturated Yucca Mountain Site*. in *High Level Radioactive Waste Management: Proceedings of the fifth annual international conference. Volume 2*. 1994.
16. Institute, J.N.C.D., *H12: Project to Establish the Scientific and Technical Basis for HLW Disposal in Japan: Supporting Report 3, Safety Assessment of the Geological Disposal System*. 2000: Japan Nuclear Cycle Development Institute.
17. Mueller, W., A. Nold, and J. Poettinger, *Kristallin-I: Conclusions from the regional investigation programme for siting a HLW repository in the crystalline basement of Northern Switzerland*. 1994, Nationale Genossenschaft fuer die

Lagerung Radioaktiver Abfaelle (NAGRA).
18. Smith, P., et al., *Safety assessment for a KBS-3H spent nuclear fuel repository at Olkiluoto.* Summary report. Posiva, 2007. **6**.
19. Verhoef, E., et al., *Outline of a disposal concept in clay.* COVRA NV Report OPERA-PG_COV008 (Vlissingen), 2011.
20. Apted, M.J. and J. Ahn, *Geological repository systems for safe disposal of spent nuclear fuels and radioactive waste*. 2010: Elsevier.
21. Baekelandt, L., J. Bel, and J. Boyazis, *SAFIR2. Safety Assessment and Feasibility Interim Report 2*. 2001, NIROND.
22. Bonin, B., *Deep geological disposal in argillaceous formations: studies at the Tournemire test site.* Journal of Contaminant Hydrology, 1998. **35**(1): p. 315-330.
23. Aoki, K., *Recent activities at underground research laboratories in Japan*. 2002.
24. Arkai, P., et al., *Composition, diagenetic and post-diagenetic alterations of a possible radioactive waste repository site: the Boda Albitic Claystone Formation, southern Hungary.* Acta Geologica Hungarica, 2000. **43**(4): p. 351-378.
25. radioactifs, S.c.n.p.l.e.d.d. and L. Johnson, *Project Opalinus Clay: safety report: demonstration of disposal feasibility for spent fuel, vitrified high-level waste and long-lived intermediate-level waste (Entsorgungsnachweis)*. 2002: NAGRA.
26. Boisson, J., *Clay Club catalogue of characteristics of argillaceous rocks, Radioactive waste management.* Nuclear Energy Agency, 2005(4436): p. 72.
27. Villar, M., *MX-80 bentonite. Thermo-hydro-mechanical characterisation performed at CIEMAT in the context of the Prototype Project.* 2005.
28. Koenen, M. and J. Griffioen, *Characterisation of the geochemical heterogeneity of the Rupel Clay Member in the Netherlands.* Netherlands Journal of Geosciences, 2016: p. 1-13.
29. Zeelmaekers, E., et al., *Qualitative and quantitative mineralogical composition of the Rupelian Boom Clay in Belgium.* Clay Minerals, 2015. **50**: p. 249-272.
30. Karnland, O., *Chemical and mineralogical characterization of the bentonite buffer for the acceptance control procedure in a KBS-3 repository*. 2010, Swedish Nuclear Fuel and Waste Management Co.
31. Jönsson, B., et al., *Structure and forces in bentonite MX-80*. 2009: Svensk kärnbränslehantering AB (SKB).
32. Baeyens, B., et al., *Aging effects in boom clay.* Radioact. Waste Manage. Nucl. Fuel Cycle, 1985. **6**(3-4): p. 409-423.
33. Henrion, P., et al., *Migration of radionuclides in Boom Clay.* Radioact. Waste Manage. Nucl. Fuel Cycle, 1985. **6**(3-4): p. 313-359.
34. Volckaert, G., et al., *Characteristics of argillaceous rocks. A catalogue of the characteristics of argillaceous rocks studied with respect to radioactive waste disposal issues: Belgium, Canada, France, Germany, Italy, Japan, Spain, Switzerland, United Kingdom and United States.* Canada, France, Germany, Italy, Japan, Spain, Switzerland, United Kingdom, and Unite States-Boom Clay,

Revision, 1997(2-05): p. 1997.
35. Wouters, L., et al., *Innovative applications of dual range Fourier transform infrared spectroscopy to analysis of Boom Clay mineralogy*, in *Aardkundige Mededelingen*. 1997. p. 159-168.
36. De Craen, M., et al., *Geochemistry of Boom Clay pore water at the Mol site.* SCK-CEN scientific report BLG-990. Waste & Disposal Department SCK-CEN (Mol, Belgium), 2004.
37. Van Keer, I. and M. De Craen, *Sedimentology and diagenetic evolution of the Boom Clay: State of the art.* Long-Term Performance Studies of the Geological Disposal of Conditioned High-Level and Long-Lived Radioactive Waste. Report to NIRAS/ONDRAF contract CCHO-98/332/KNT, 2001. **90**: p. 1042.
38. De Craen, M., L. Wang, and E. Weetjens, *Natural evidence on the long-term behaviour of trace elements and radionuclides in the Boom Clay.* SCK• CEN report R-3926, Mol, Belgium, 2004.
39. Tournassat, C., et al., *Chapter 1 - Surface Properties of Clay Minerals*, in *Developments in Clay Science*, C.I.S.I.C.B. Christophe Tournassat and B. Faqpza, Editors. 2015, Elsevier. p. 5-31.
40. Holmboe, M., S. Wold, and M. Jonsson, *Porosity investigation of compacted bentonite using XRD profile modeling.* Journal of Contaminant Hydrology, 2012. **128**(1): p. 19-32.
41. Lagaly, G. and I. Dékány, *Chapter 8 - Colloid Clay Science*, in *Developments in Clay Science*, B. Faïza and L. Gerhard, Editors. 2013, Elsevier. p. 243-345.
42. Ruedrich, J., et al., *Moisture expansion as a deterioration factor for sandstone used in buildings.* Environmental Earth Sciences, 2011. **63**(7): p. 1545-1564.
43. Norrish, K., *The swelling of montmorillonite.* Discussions of the Faraday society, 1954. **18**: p. 120-134.
44. Pansu, M. and J. Gautheyrou, *Handbook of soil analysis: mineralogical, organic and inorganic methods*. 2007: Springer Science & Business Media.
45. Weber, C., *On the Characterization of Electric Double Layers of Clay Minerals and Their Relevance for Macroscopic Transport Phenomena: Zur Charakterisierung Von Elektrischen Doppelschichten Von Tonmineralen und Deren Relevanz Für Makroskopische Transportphänomene*. 2015.
46. Sposito, G., et al., *Surface geochemistry of the clay minerals.* Proceedings of the National Academy of Sciences, 1999. **96**(7): p. 3358-3364.
47. 迪夫, 岡., *電気二重層キャパシタと蓄電システム*. 2001: 日刊工業新聞社.
48. Marques Fernandes, M., B. Baeyens, and C. Beaucaire, *8 - Radionuclide retention at mineral–water interfaces in the natural environment*, in *Radionuclide Behaviour in the Natural Environment*. 2012, Woodhead Publishing. p. 261-301.
49. Borisover, M. and J.A. Davis, *Chapter 2 - Adsorption of Inorganic and Organic Solutes by Clay Minerals*, in *Developments in Clay Science*, C.I.S.I.C.B.

Christophe Tournassat and B. Faqpza, Editors. 2015, Elsevier. p. 33-70.
50. Fenter, P.A., *Applications of synchrotron radiation in low-temperature geochemistry and environmental sciences*. Vol. 49. 2002: Geochemical Society.
51. Wu, C.-H., S.-L. Lo, and C.-F. Lin, *Competitive adsorption of molybdate, chromate, sulfate, selenate, and selenite on γ-Al 2 O 3.* Colloids and Surfaces A: Physicochemical and Engineering Aspects, 2000. **166**(1): p. 251-259.
52. Wu, C.-H., et al., *Modeling competitive adsorption of molybdate, sulfate, selenate, and selenite using a Freundlich-type multi-component isotherm.* Chemosphere, 2002. **47**(3): p. 283-292.
53. Wu, C.-H., et al., *Modeling competitive adsorption of molybdate, sulfate, and selenate on γ-Al 2 O 3 by the triple-layer model.* Journal of colloid and interface science, 2001. **233**(2): p. 259-264.
54. Zhang, P. and D.L. Sparks, *Kinetics of selenate and selenite adsorption/desorption at the goethite/water interface.* Environmental Science & Technology, 1990. **24**(12): p. 1848-1856.
55. Sheindorf, C., M. Rebhun, and M. Sheintuch, *Organic pollutants adsorption from multicomponent systems modeled by Freundlich type isotherm.* Water Research, 1982. **16**(3): p. 357-362.
56. Takeno, N., *Atlas of Eh-pH diagrams.* Geological survey of Japan open file report, 2005. **419**: p. 102.
57. De Cannière, P., et al., *Behaviour of selenium in Boom Clay.* State-of-the-art report, 2010: p. 328.
58. Boult, K.A., et al., *Towards an understanding of the sorption of U(VI) and Se(IV) on sodium bentonite.* Journal of Contaminant Hydrology, 1998. **35**(1): p. 141-150.
59. Sato, H. and S. Miyamoto, *Diffusion behaviour of selenite and hydroselenide in compacted bentonite.* Applied Clay Science, 2004. **26**(1): p. 47-55.
60. Wu, T., et al., *Salt effects on Re(VII) and Se(IV) diffusion in bentonite.* Applied Clay Science, 2017. **141**: p. 104-110.
61. Maes, N., et al., *The assessment of electromigration as a new technique to study diffusion of radionuclides in clayey soils.* Journal of Contaminant Hydrology, 1999. **36**(3): p. 231-247.
62. Maes, N., et al., *The use of electromigration as a qualitative technique to study the migration behaviour and speciation of uranium in the Boom Clay.* Radiochimica Acta, 2002. **90**(9-11): p. 741-746.
63. Beauwens, T., et al., *Studying the migration behaviour of selenate in Boom Clay by electromigration.* Engineering geology, 2005. **77**(3): p. 285-293.
64. Bruggeman, C., et al., *Iodine retention and migration behaviour in Boom clay.* External report of Belgian Nuclear Research Centre, SCK· CEN-ER-119, 2010.
65. Vermunt, T., *Selenium anions diffusion in bentonite in the presence of silicates*. 2016, Delft University of Technology.
66. Carter, P., *The influence of competition between selenate and metasilicate ions on their migration behavior in bentonite*. 2015, Delft University of Technology.
67. Zappey, J., *Radionuclide migration in the nearfield of geological respository*.

2013, Delft University of Technology.
68. Bruggeman, C., *Assessment of the geochemical behaviour of selenium oxyanions under Boom Clay geochemical conditions.* 2006.
69. Arnold, P., et al., *A numerical and reliability-based investigation into the technical feasibility of a Dutch.* 2015.
70. De Craen, M., et al., *High sulphate concentrations in squeezed Boom Clay pore water: evidence of oxidation of clay cores.* Physics and Chemistry of the Earth, Parts A/B/C, 2004. **29**(1): p. 91-103.
71. De Craen, M., et al., *Overview of the oxidation around galleries in Boom Clay (Mol, Belgium)–status 2008.* SCK-CEN report ER-189, 2011.
72. Idemitsu, K., et al., *Diffusion behavior of selenite in purified bentonite.* Progress in Nuclear Energy, 2016. **92**: p. 279-285.
73. Sato, H., M. Yui, and H. Yoshikawa, *Diffusion behavior for Se and Zr in sodium-bentonite.* MRS Online Proceedings Library Archive, 1994. **353**.
74. Chan, Y.T., et al., *Adsorption mechanism of selenate and selenite on the binary oxide systems.* water research, 2009. **43**(17): p. 4412-4420.
75. Constantino, L.V., et al., *Sorption-desorption of selenite and selenate on Mg-Al layered double hydroxide in competition with nitrate, sulfate and phosphate.* Chemosphere, 2017. **181**: p. 627-634.
76. Hu, S., W. Yan, and J. Duan, *Polymerization of silicate on TiO2 and its influence on arsenate adsorption: An ATR-FTIR study.* Colloids and Surfaces A: Physicochemical and Engineering Aspects, 2015. **469**: p. 180-186.
77. Hiemstra, T., M.O. Barnett, and W.H. van Riemsdijk, *Interaction of silicic acid with goethite.* Journal of Colloid and Interface Science, 2007. **310**(1): p. 8-17.
78. Ochs, M., et al., *A quantitative model for ion diffusion in compacted bentonite.* Radiochimica Acta, 1998. **82**(s1): p. 437-444.
79. Ochs, M., et al., *An integrated sorption–diffusion model for the calculation of consistent distribution and diffusion coefficients in compacted bentonite.* Journal of Contaminant Hydrology, 2001. **47**(2): p. 283-296.
80. Sato, H., et al., *Effect of dry density on diffusion of some radionuclides in compacted sodium bentonite.* Journal of Nuclear Science and Technology, 1992. **29**(9): p. 873-882.
81. Kim, H.-T., et al., *Diffusivities for ions through compacted Na-bentonite with varying dry bulk density.* Waste Management, 1993. **13**(4): p. 303-308.
82. Jenni, A., et al., *In situ interaction between different concretes and Opalinus Clay.* Physics and Chemistry of the Earth, Parts A/B/C, 2014. **70**: p. 71-83.
83. Wang, L., D. Jacques, and P. De Cannière, *Effects of an alkaline plume on the Boom Clay as a potential host formation for geological disposal of radioactive waste.* External Report SCK• CEN-ER-28, SCK• CEN, Belgium, 2010.
84. Kuila, U. and M. Prasad, *Specific surface area and pore-size distribution in clays and shales.* Geophysical Prospecting, 2013. **61**(2): p. 341-362.
85. Gaboreau, S., et al., *15 years of in situ cement–argillite interaction from Tournemire URL: Characterisation of the multi-scale spatial heterogeneities of pore space evolution.* Applied Geochemistry, 2011. **26**(12): p. 2159-2171.

86. Liu, S., et al., *Conceptual model analysis of interaction at a concrete–Boom Clay interface.* Physics and Chemistry of the Earth, Parts A/B/C, 2014. **70**: p. 150-159.
87. Kosakowski, G. and U. Berner, *The evolution of clay rock/cement interfaces in a cementitious repository for low-and intermediate level radioactive waste.* Physics and Chemistry of the Earth, Parts A/B/C, 2013. **64**: p. 65-86.
88. Karnland, O., S. Olsson, and U. Nilsson, *Mineralogy and sealing properties of various bentonites and smectite-rich clay materials*. 2006: SKB Stockholm.